

AD-A188 325

INTEGRATED OPTICAL SYNTHETIC APERTURE RADAR PROCESSOR
(U) UNIVERSITY OF SOUTHERN CALIFORNIA LOS ANGELES
OPTICAL MATERIA. A R TANGUAY SEP 87 USC/OMDL-1681

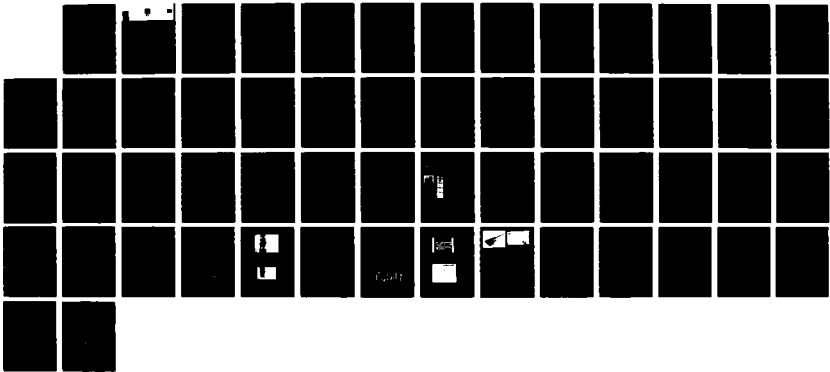
1/1

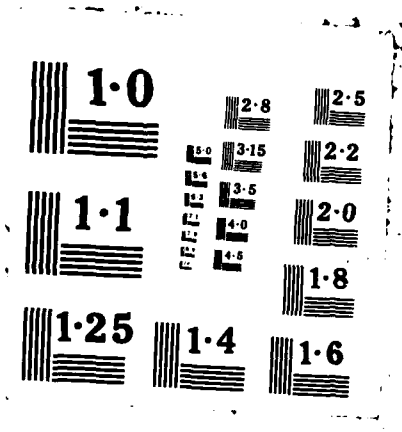
UNCLASSIFIED

AFOSR-TR-87-1594 AFOSR-84-8352

F/G 17/9

NL





AD-A188 325



2

UNIVERSITY OF SOUTHERN CALIFORNIA

USC OMDL 1601

INTEGRATED OPTICAL SYNTHETIC APERTURE
RADAR PROCESSOR
AFOSR-84-0352

FINAL RESEARCH REPORT
(RESEARCH PERIOD: 09/01/84 - 11/30/85)

Approved for public release;
distribution unlimited.

Submitted To:

Air Force Office of Scientific Research
Electronics and Materials Science Division
AFOSR/NE

Bolling AFB, Bldg. 410
Washington, D.C. 20332
Attn: Dr. C. Lee Giles

SDTIC
ELECTE
NOV 20 1987
H

Submitted By:

Dr. Armand R. Tanguay, Jr.
Optical Materials and Devices Laboratory
University of Southern California
University Park, MC-0483
Los Angeles, California 90089



OFFICE OF MATERIALS DEVELOPMENT

UNCLASSIFIED

SECURITY CLASSIFICATION OF THIS PAGE

188 325

REPORT DOCUMENTATION PAGE

1a. REPORT SECURITY CLASSIFICATION UNCLASSIFIED		1b. RESTRICTIVE MARKINGS	
2a. SECURITY CLASSIFICATION AUTHORITY		3. DISTRIBUTION/AVAILABILITY OF REPORT APPROVED FOR PUBLIC RELEASE: DISTRIBUTION UNLIMITED	
2b. DECLASSIFICATION/DOWNGRADING SCHEDULE			
4. PERFORMING ORGANIZATION REPORT NUMBER(S) USC OMDL-1601		5. MONITORING ORGANIZATION REPORT NUMBER(S) AFOSR-TR- 87-1594	
6a. NAME OF PERFORMING ORGANIZATION UNIVERSITY OF SOUTHERN CALIFORNIA	6b. OFFICE SYMBOL <i>(If applicable)</i>	7a. NAME OF MONITORING ORGANIZATION AIR FORCE OFFICE OF SCIENTIFIC RESEARCH	
6c. ADDRESS (City, State and ZIP Code) UNIVERSITY OF SOUTHERN CALIFORNIA UNIVERSITY PARK, MC-0483 LOS ANGELES, CALIFORNIA 90089-0483		7b. ADDRESS (City, State and ZIP Code) AFOSR/NE BUILDING 410 BOLLING AFB, DC 20332	
8a. NAME OF FUNDING/SPONSORING ORGANIZATION <i>Same as 7a</i>	8b. OFFICE SYMBOL <i>(If applicable)</i>	9. PROCUREMENT INSTRUMENT IDENTIFICATION NUMBER AFOSR-84-0352	
8c. ADDRESS (City, State and ZIP Code) <i>Same as 7b</i>		10. SOURCE OF FUNDING NOS.	
		PROGRAM ELEMENT NO. <i>61102F</i>	TASK NO. <i>B4</i>
		PROJECT NO. <i>2305</i>	WORK UNIT NO.
11. TITLE (Include Security Classification) INTEGRATED OPTICAL SYNTHETIC APERTURE RADAR PROCESSOR			
12. PERSONAL AUTHOR(S) DR. ARMAND R. TANGUAY, JR.			
13a. TYPE OF REPORT FINAL REPORT	13b. TIME COVERED FROM 09/01/84 TO 11/30/85	14. DATE OF REPORT (Yr., Mo., Day) 1987, SEPTEMBER	15. PAGE COUNT 49
16. SUPPLEMENTARY NOTATION			
17. COSATI CODES		18. SUBJECT TERMS (Continue on reverse if necessary and identify by block number)	
FIELD	GROUP	SUB. GR.	
19. ABSTRACT (Continue on reverse if necessary and identify by block number)			
<p>The principal objective of this research program was initiation of the development of a compact, rugged, low-cost, low-power optical synthetic aperture radar processor for real-time image formation aboard airborne and spaceborne platforms.</p> <p>The extremely high computational burden associated with SAR imaging has thus far limited the usefulness of the technique to non-real-time applications from fixed platform bases. Existing real-time digital and optical techniques are in general too bulky, power consumptive, and expensive for broad applicability, particularly in space-confined mobile environments. The integrated optics approach described herein provides a powerful solution with which to circumvent these limitations.</p> <p>The key to this novel optical processing concept is the use of planar optical waveguide technology (which allows the integration of optical components in a single substrate) in conjunction with a time-and-space integrating architecture (which allows two-dimensional</p>			
20. DISTRIBUTION/AVAILABILITY OF ABSTRACT UNCLASSIFIED/UNLIMITED <input checked="" type="checkbox"/> SAME AS RPT. <input type="checkbox"/> DTIC USERS <input type="checkbox"/>		21. ABSTRACT SECURITY CLASSIFICATION UNCLASSIFIED	
22a. NAME OF RESPONSIBLE INDIVIDUAL <i>Giles</i>		22b. TELEPHONE NUMBER <i>(202) 767-4931</i>	22c. OFFICE SYMBOL <i>NE</i>

19. ABSTRACT (continued)

processing to be performed in a quasi-planar optical structure). An additional novel feature is the utilization of partial waveguide confinement to allow uniform light emission vertically out of the plane of the integrated optical substrate and onto a two-dimensional time-integrating detector.

The unique features of this approach are:

1. The implementation of two-dimensional SAR processing utilizing both integrated optics and time-and-space integration
2. Vertical integration of an optical waveguide with a CCD image sensor
3. The use of in-plane parallel channel or rib waveguiding to retain lateral image integrity
4. Surface acoustic wave generation in optical waveguide materials with slow acoustic velocity to achieve large effective radar apertures
5. Selective partial waveguide confinement of channelized light in an integrated optics chip

The novel integrated optics architecture described in this report is potentially programmable to allow additional types of computational algorithms to be implemented. These include the compensation of SAR images for changes in platform variables and geometric distortions, two-dimensional correlation, convolution, and Fourier transform operations, and real time computation of ambiguity functions.

INTEGRATED OPTICAL SYNTHETIC APERTURE RADAR PROCESSOR

TABLE OF CONTENTS

<u>SECTION</u>	<u>PAGE</u>
LIST OF FIGURES	i
LIST OF APPENDICES	ii
ABSTRACT	1
1. INTRODUCTION	3
2. BACKGROUND OF RESEARCH PROGRAM	5
3. STATEMENT OF TECHNICAL OBJECTIVES	8
4. SUMMARY OF RESEARCH PROGRAM	9
5. PUBLICATIONS	20
5.1 PUBLISHED MANUSCRIPTS	20
5.2 CONFERENCE PRESENTATIONS	20
6. SCIENTIFIC PERSONNEL	21
7. REFERENCES	22

Accession For	
NTIS GRA&I	<input checked="" type="checkbox"/>
DTIC TAB	<input type="checkbox"/>
Unannounced	<input type="checkbox"/>
Justification	
By	
Distribution/	
Availability Codes	
Avail and/or	
Dist	Special
A-1	



INTEGRATED OPTICAL SYNTHETIC APERTURE RADAR PROCESSOR

LIST OF FIGURES

<u>FIGURE</u>		<u>PAGE</u>
Fig. 1.	Acoustooptic synthetic aperture radar processor utilizing discrete components [1]. The top view shows the range focus due to the linear fm SAR return; the side view shows the vertical expansion in a given range bin required for time integration on the CCD array detector.	6
Fig. 2.	Schematic diagram of the Integrated Optical Synthetic Aperture Radar Processor, as described in Sect. 4 of the text.	10
Fig. 3.	Waveguide outcoupling from a rib or channel waveguide by uniform periodic modulation of the waveguide surface.	15
Fig. 4.	Waveguide outcoupling from a rib or channel waveguide by nonuniform periodic modulation of the waveguide surface to compensate for outcoupling loss in the direction of propagation.	16

INTEGRATED OPTICAL SYNTHETIC APERTURE RADAR PROCESSOR

LIST OF APPENDICES

<u>APPENDIX</u>	<u>PAGE</u>
Appendix A D. Psaltis and K. Wagner, "Real-Time Optical Synthetic Aperture Radar (SAR) Processor", Opt. Eng. 21(5), 822-828, (1982).	24
Appendix B D. Psaltis, M. Haney, and K. Wagner, "Real Time Synthetic Aperture Radar Processing", Proc. NASA Conference on Optical Information Processing for Aerospace Applications. II, Langley, Virginia, (1983).	31
Appendix C I. Abramov, Y. Owechko, A. R. Tanguay, Jr., and T. J. Bicknell, "Real Time Synthetic Aperture Image Formation Utilizing an Electrooptic Spatial Light Modulator", Proc. NASA Spaceborne Imaging Radar Symposium, Jet Propulsion Laboratory Publication No. 83-11, (1983).	45

INTEGRATED OPTICAL SYNTHETIC APERTURE RADAR PROCESSOR

ABSTRACT

The principal objective of this research program was initiation of the development of a compact, rugged, low-cost, low-power optical synthetic aperture radar processor for real-time image formation aboard airborne and spaceborne platforms.

The extremely high computational burden associated with SAR imaging has thus far limited the usefulness of the technique to non-real-time applications from fixed platform bases. Existing real-time digital and optical techniques are in general too bulky, power consumptive, and expensive for broad applicability, particularly in space-confined mobile environments. The integrated optics approach described herein provides a powerful solution with which to circumvent these limitations.

The key to this novel optical processing concept is the use of planar optical waveguide technology (which allows the integration of optical components in a single substrate) in conjunction with a time-and-space integrating architecture (which allows two-dimensional processing to be performed in a quasi-planar optical structure). An additional novel feature is the utilization of partial waveguide confinement to allow uniform light emission vertically out of the plane of the integrated optical substrate and onto a two-dimensional time-integrating detector.

The unique features of this approach are:

1. The implementation of two-dimensional SAR processing utilizing both integrated optics and time-and-space integration
2. Vertical integration of an optical waveguide with a CCD image sensor
3. The use of in-plane parallel channel or rib waveguiding to retain lateral image integrity
4. Surface acoustic wave generation in optical waveguide materials with slow acoustic velocity to achieve large effective radar apertures
5. Selective partial waveguide confinement of channelized light in an integrated optics chip

The novel integrated optics architecture described in this report is potentially programmable to allow additional types of computational algorithms to be implemented. These include the compensation of SAR images for changes in platform variables and geometric distortions, two-dimensional correlation, convolution, and Fourier transform operations, and real time computation of ambiguity functions.

INTEGRATED OPTICAL SYNTHETIC APERTURE RADAR PROCESSOR

1. INTRODUCTION

Synthetic Aperture Radar (SAR) is a very powerful imaging technique that allows the formation of high resolution images using radar-frequency probes. In a conventional real aperture imaging system, the resolution is inversely proportional to the aperture of the imaging system. Thus, improved resolution can only be obtained at the expense of a large radar antenna, which is in general too bulky to carry aboard an airborne or spaceborne platform. In many cases, the desired resolution would require antennas of truly massive size, which are impractical for any platform. In a SAR system, on the other hand, the resolution is approximately equal to the antenna aperture in the azimuth direction and it is entirely independent of the antenna aperture in the range dimension.

The signal detected by a SAR system, however, is not a focused image; extensive processing is required to form the image from the received signal. Film based optical processing systems have been very effectively used in the past twenty-five years to perform the required SAR processing. More recently, digital computers have been also used extensively in SAR image formation. However, film based optical processors and high speed minicomputers are not suitable for real time image formation aboard the radar platform because of computational speed limitations, and also because of the large size, weight and power consumption of such systems. Recently, optical techniques have been demonstrated at both Caltech and USC that allow real time SAR image formation with relatively compact and power efficient optical systems. These systems were implemented with discrete components [1,2,3; see also Appendices A, B, C]. In one approach [1,2], an acousto-optic cell was employed to input each radar return into a time-and-space integrating optical architecture comprised of several lenses, a CCD area array detector, and a proximity-coupled mask. In this approach, the range compression derives from self-focusing of the chirped radar pulse, while azimuth compression is achieved by mask multiplication and sequential time-integration on the CCD array, operated in the shift-and-add mode. This architecture is explained in more detail in Section 2 and in Appendices A and B. In the second approach [3], the incoming radar return at a given azimuth coordinate is written onto one column of a two-dimensional real-time spatial light modulator such as the PROM (Pockels Readout Optical Modulator) [4]. Sequential radar return pulses are written onto adjacent columns. This input function can be performed by a serial-to-parallel converter such as the Linear Array Total Internal Reflection Spatial Light Modulator [5]. Range and azimuth compression are then both achieved in

parallel by means of an anamorphic imaging system, which relies on the self-focusing properties of the radar return Fresnel zone plate in both dimensions. Further details are provided in Appendix C.

A further reduction in the size, weight, power and cost requirements of a real-time SAR processor can be realized if these optical components could be integrated onto a single optical waveguide substrate. The value of such an achievement can be immediately realized by comparison of several pertinent characteristics of existing real-time SAR processors. For example, a current digital implementation comprises the equivalent of two vertical six-foot equipment racks, weighs about 1500 pounds, consumes from one to five kilowatts of power, and costs several hundred thousand dollars [6]. The optical implementations described above are of order one-half cubic meter in size, weigh about twenty pounds, consume less than five watts of power, and cost about ten thousand dollars. The integrated optical approach described herein will be of order four cubic inches in size, weigh about one-half pound, consume less than 200 milliwatts of power, and cost no more than a few hundred dollars in quantity.

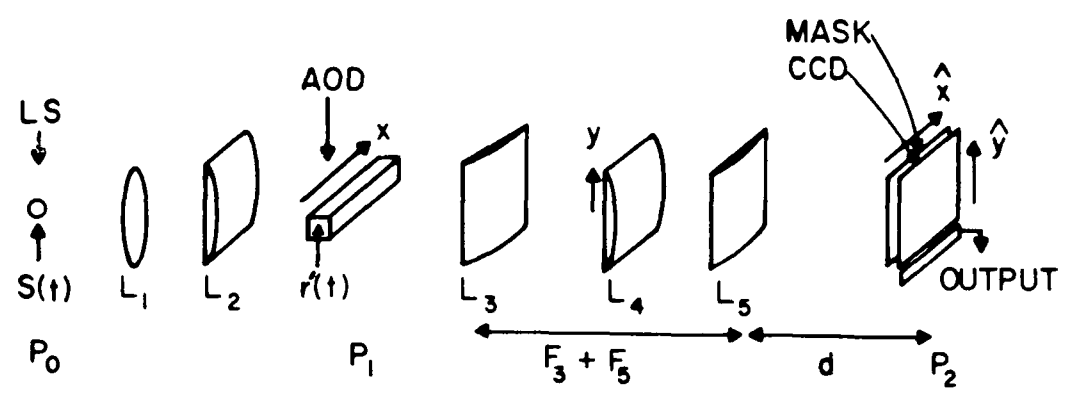
The novel aspect of the proposed research is the computation of two-dimensional operations using integrated optics. The formation of a SAR image is inherently a two-dimensional operation, in that both azimuth and range information must be extracted from the microwave radar returns. Integrated optics, on the other hand, is a planar technology usually thought suited for only one-dimensional processing functions (and to which it has been recently applied [7,8,9]). In this report, we describe initial feasibility studies of the implementation of two-dimensional processing with an integrated optics structure, using the time-and-space integrating architecture [10]. With this method, two-dimensional data is encoded in time and one spatial coordinate, and the data is processed by a combination of spatial and temporal integration within the optical system to achieve the requisite range and azimuth compression functions. Although only one spatial coordinate is utilized, it is possible to accomplish extremely complicated two-dimensional signal processing functions such as SAR image formation within the confines of a planar integrated optics structure by means of a novel architecture that involves the vertical extraction of image intensity from an array of parallel waveguides. Temporal integration is provided by a proximity-coupled area array CCD detector. This concept is described more fully in Section 4, Summary of Research Program.

2. BACKGROUND OF THE RESEARCH PROGRAM

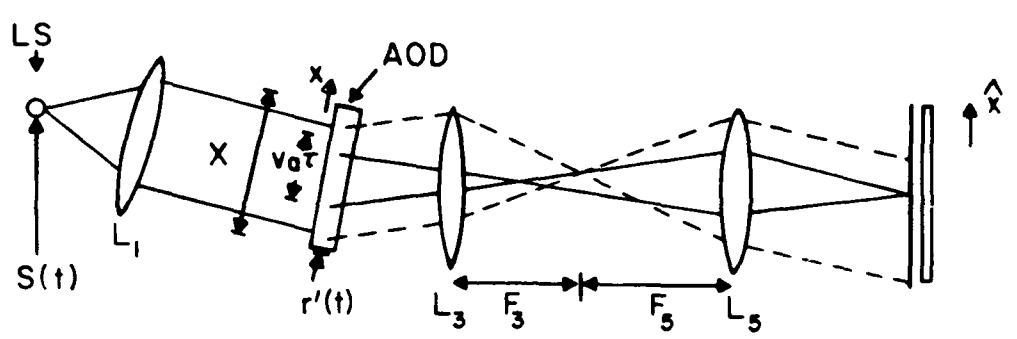
A schematic diagram of the aforementioned discrete acoustooptic SAR processor [1,2] is shown in Fig. 1. The theory of operation of this processor is described in detail in Appendix A, and a recent experimental demonstration is presented in Appendix B. Briefly, the input to the processor is the radar signal return, which is applied to the acoustooptic device (AOD) in Fig. 1. The light diffracted by the AOD is expanded uniformly in the vertical direction and it self-focuses horizontally due to the linear FM pulse shape of the radar signal. The self-focusing of the diffracted light produces a focused radar image in the range dimension only. The range focused image is multiplied by a fixed two-dimensional mask, on which the azimuth phase history is recorded, and the product is detected on a two-dimensional CCD detector array. The photogenerated charge on the CCD is continuously transferred step-wise in the vertical direction during the exposure of the device to light. The relative motion between the signal on the CCD and the stationary mask results in the required correlation in the azimuth direction. Thus the output video signal from the CCD is the two-dimensional, focused radar image. In this architecture the simultaneous use of time and space integration allows the two-dimensional image forming operation to be implemented with a one-dimensional AOD as the input transducer. This implementation utilizes two transverse spatial coordinates; the second dimension is needed to uniformly expand the light in order to address the two-dimensional mask and CCD. In an integrated optics (IO) implementation of such a processor, a method must therefore be found for addressing the mask and CCD in a planar geometry. This method is described in Section 4.

The term "integrated optics" refers to the technology with which optical and electro-optical components can be integrated on a single substrate. The components that we are interested in integrating are the light source, detector, lenses, waveguides, and modulators. Therefore, in selecting a substrate material, consideration must be given to the technology that is available for fabricating each of the individual components with this material. At present, no one material exists within which all the required components can be fabricated. Consequently, fully integrated optical systems are not yet feasible. The material most commonly used thus far is LiNbO_3 , in which optical waveguides, lenses, electrooptic and acoustooptic (SAW) modulators can be monolithically fabricated. The laser diode source and detector are typically butt-coupled at the two ends of the integrated optics chip. Materials such as GaAs show promise for full integration in future years.

To date, integrated optical (or at least hybrid-integrated guided wave optical) spectrum analyzers, one-dimensional correlators, and simple vector-matrix multipliers have been demonstrated. One of the frequently stated limitations of integrated optics technol-



TOP VIEW



SIDE VIEW

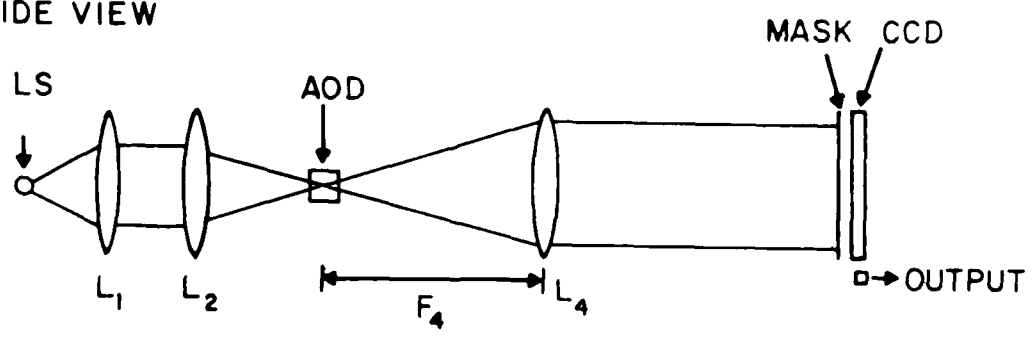


Fig. 1 Acoustooptic synthetic aperture radar processor utilizing discrete components [1]. The top view shows the range focus due to the linear fm SAR return; the side view shows the vertical expansion in a given range bin required for time integration on the CCD array detector.

ogy with regard to optical information processing is the fact that it is a planar technology and therefore not applicable to two-dimensional processing problems. The time and space integrating method combined with in-plane waveguiding that is described in Section 4 provides a powerful and elegant solution to this problem.

3. STATEMENT OF TECHNICAL OBJECTIVES

The full-scale development of an Integrated Optical Synthetic Aperture Radar Processor involves a wide range of definable tasks, including design, fabrication, and characterization of a hybrid-integrated laser diode, a waveguide surface acoustic wave transducer, several integrated optical collimation lenses, a rib or channel waveguide array, SAR azimuth compression masks, a charge-coupled device (CCD) to waveguide interface, system integration, device characterization, demonstration of real-time SAR image formation, and the exploration of applications to other significant problems amenable to solution by optical processing algorithms. In order to accomplish these tasks, a collaborative effort between research groups at the University of Southern California (Principal Investigator: Professor Armand R. Tanguay, Jr.) and the California Institute of Technology (Principal Investigator: Professor Demetri Psaltis) was proposed, and implemented by two separate research contracts. In general, the source hybridization, surface acoustic wave device design and fabrication, and SAR algorithm mask design were designed to be the responsibility of Caltech, while the integrated optical lens design and fabrication, rib or channel waveguide design and fabrication, and CCD detector interface were designed to be the responsibility of USC. System integration, device characterization and analysis, and real time SAR image formation tasks were proposed to be shared by both institutions, as were the investigation of other optical processing applications of the novel architecture.

Our specific goal for this initial 15 month program (covering the research period from 9/1/84 through 11/30/85) was the demonstration of the feasibility of the approach, and solution of several key issues regarding its potential implementation. In Section 4, the specific research task items that were pursued during the course of the research are described.

4. SUMMARY OF RESEARCH PROGRAM

Description of the Processor

The proposed Integrated Optical (IO) SAR processor is shown schematically in Fig. 2. It consists of a single crystal substrate, the surface of which has been modified to change the index of refraction of a thin layer near the surface and thus form a planar waveguide. Light from a semiconductor laser (attached to the IO chip) is butt-coupled at the left and is guided in the vertical direction along the surface of the chip. In the horizontal direction the light is diverging, and waveguide-lens L1 is used to collimate it. A surface acoustic wave (SAW) is launched along the top surface of the chip in a direction approximately perpendicular to the direction of propagation of the light. The SAW is modulated by the radar signal and causes a portion of the incident light to be diffracted. Lens L2 focuses the diffracted light at plane P0. The one dimensional light distribution at plane P0 is the radar image focused in the range dimension only. An array of rib waveguides is fabricated on the IO chip after plane P0. The rib waveguides serve a two-fold purpose. First, they retain the integrity of the range focused image after plane P0 (i.e. they prevent the image from going out of focus as it propagates away from plane P0). Second, they expand the range focused-image in the plane of the chip so that the two-dimensional mask and CCD that are part of the acoustooptic SAR processor can be addressed. This is accomplished by making the top surface of rib waveguides leaky, so that a portion of the light escapes upwards as it travels in each waveguide. Several methods for achieving this are discussed later. The mask and CCD are then placed in contact with the surface of the IO chip so that the escaping light will be multiplied by the transmittance of the mask and detected by the CCD. The radar image is focused in the second (azimuth) direction by transferring and integrating the photogenerated charge on the CCD precisely as in the the acoustooptic SAR processor described in Appendices A and B.

A. Surface Acoustic Wave Device Fabrication

SAW devices have been fabricated in a wide variety of crystals. Most of the SAW/IO devices are fabricated with LiNbO_3 at the current time, primarily because optical waveguides and other optical components can also be fabricated easily in LiNbO_3 . However, LiNbO_3 is not optimum for the SAR application because the acoustic velocity is too high, and this limits the allowable acoustic delay (and hence the range delay in the SAR processor) to approximately 1 microsecond. In the SAR application, an acoustic delay time of at least 50 microseconds is required in order to generate sufficient range coverage. We investigated the properties of a range of single crystal substrate materials with low acoustic surface wave velocities, to determine those in which both SAW devices and opti-

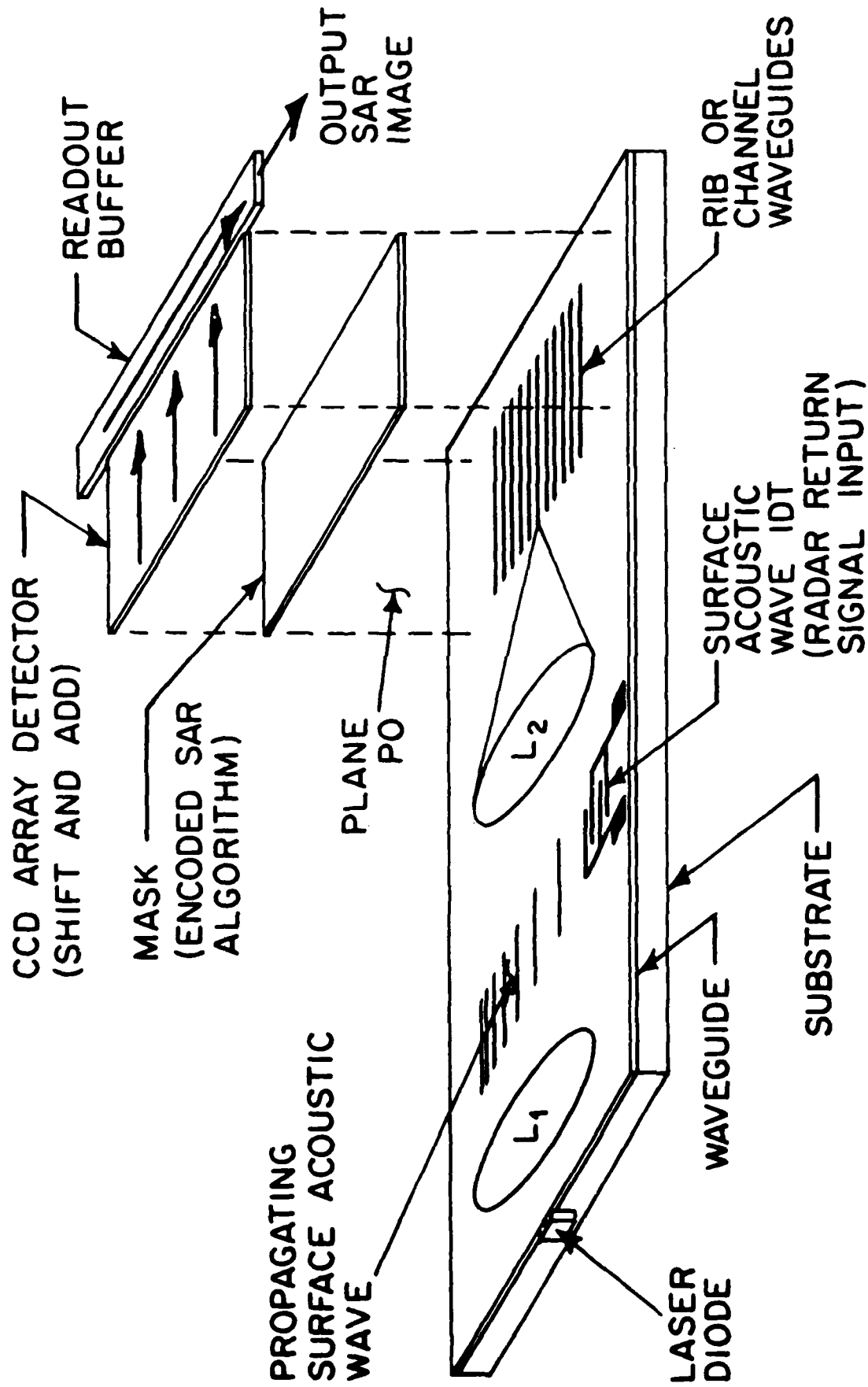


Fig. 2 Schematic diagram of the Integrated Optical Synthetic Aperture Radar Processor, as described in Sect. 4 of the text.

cal waveguides can be fabricated. Although tellurium dioxide (TeO_2) has a significantly lower surface acoustic wave velocity (shear wave) than that of LiNbO_3 , current technology does not seemingly permit straightforward and reproducible fabrication of large area waveguides in this material. This appears to be primarily due to a lack of investigative effort moreso than to any fundamental reason.

As a direct result of this survey, it was determined that LiNbO_3 is a more attractive material for purposes of concept demonstration. As such, we decided to fabricate all proof of concept device structures and substructures on LiNbO_3 substrates.

B. Integrated Optical Lens Fabrication

A second key component of the Integrated Optical SAR Processor involves the fabrication of a collimating lens for the laser diode, and a focusing lens for the acoustooptic device (to significantly shorten the focal lengths that characterize typical linear FM chirp waveforms in a SAW transducer). A large number of investigators have examined the lens fabrication issue, and a range of implementable solutions exists, including both geodesic and Luneberg lenses. Since this component has been thoroughly investigated by others, we proposed to postpone examination of the specific issues involved in such a lens design until all other critical issues that bear on proof-of-concept have been satisfactorily demonstrated. During the initial program period, we did however search the literature for previous results that bear directly on our task, examined questions related to lens f-number that derive from appropriate free propagation-to-confined waveguide mode propagation, and incorporated the results of these studies into design of the optimum acoustooptic cell and parallel rib waveguide structure.

During the course of the literature survey, we became aware of an elegant and potentially profound advance in the fabrication of integrated lenses and lens arrays in LiNbO_3 by the titanium indiffused- proton exchange (TIPE) process [11]. Nearly diffraction limited performance was obtained in several experimental demonstrations of lithographically defined microlenses and microlens arrays, including lenses of large aperture [11]. These results are of immediate significance to our current research, as they point to greatly simplified but high performance large aperture lenses as required by the IOSAR processor geometry. In particular, the extraordinary large refractive index changes induced by the TIPE process imply much lower curvature lens surfaces for the same f-number, which in turn reduces the aberrations as well as the overall size of the processor.

C. Rib/Channel Waveguide Fabrication

As shown in Fig. 2, an essential feature of the integrated optical SAR image formation concept is the fabrication of a parallel array of either rib or channel waveguides that simultaneously preserve the range information while allowing the azimuth correlation to be

performed by the shift-and-add CCD detector. A number of key issues pertain to the successful implementation of such a novel structure (unique primarily in that the individual waveguides are to be designed to couple a given amount of light per unit length out of the top of the guide, through the proximity-coupled mask and onto the CCD array detector). These issues include the minimization of cross-talk between individual ribs or channels, the choice of either ribs or channels for array implementation, the coupling efficiency from the mesa containing the integrated lens into each individual rib/channel (each of which represents an independent range bin), the minimization of sidewall irregularities that can lead to scattered light loss (and a consequent reduction in both outcoupling uniformity and overall signal-to-noise ratio), and the uniform fabrication of large area arrays (of order $1 \times 1 \text{ cm}^2$) with very large numbers of independent ribs or channels (of order 1000). Further, the fabrication process chosen must be compatible with a method of outcoupling from the array that can be produced with minimal degradation of the array channel separation characteristics. Methods of waveguide outcoupling explored during the contract period are described in the next Section (Waveguide Outcoupling Techniques).

The first step in the development of a waveguide array is the successful implementation of uniform, low loss slab waveguides. In the initial stages of the program, numerous slab waveguides were fabricated in LiNbO_3 y-cut, z-propagating substrates by standard Ti (titanium) indiffusion techniques [12]. Waveguide quality was examined by incoupling experiments utilizing rutile prism coupling, fiber butt-coupling, and end-fire coupling techniques. In all cases, the coupling was successful, and low scatter, low loss waveguides were achieved.

The second critical step in the fabrication of a parallel waveguide array is the development of a suitable high resolution microlithography process. We successfully utilized a liftoff process to fabricate high resolution channel waveguides in LiNbO_3 from a set of masks obtained from Allied-Amphenol Fiber Optics Products Division. One mask contained separate $3 \mu\text{m}$, $5 \mu\text{m}$, $7 \mu\text{m}$, and $9 \mu\text{m}$ straight waveguides 1 cm in length in conjugation with a two-port directional coupler with $5 \mu\text{m}$ channels and a $2 \mu\text{m}$ gap. Each of the channels, as well as the directional coupler, were shown to be of high quality by means of fiber butt-coupling. A second mask contained a 1 cm long Mach-Zender interferometer with $5 \mu\text{m}$ channels and a $3 \mu\text{m}$ area of common intersection, which was also demonstrated to be functional.

Analysis of the tradeoffs between rib and channel waveguides draws one to the conclusion that although channel waveguide arrays are potentially much easier to fabricate, rib waveguides may prove far more advantageous for our application due to the low values of Δn obtainable from Ti-indiffusion in LiNbO_3 and the correspondingly large

between-channel gaps required to assure effective isolation. Consequently, we ordered a Commonwealth Scientific 3 cm ion source and power supply, to be incorporated into our existing Sloan magnetron sputtering system for evaluation of the feasibility of fabricating large area arrays of high resolution ($8\ \mu\text{m}$ ribs with $2\ \mu\text{m}$ gaps) rib waveguides. Such an array would contain 1000 such ribs (range channels) in 1 cm of waveguide cross-section.

Finally, in support of our efforts to upgrade our capacity for ion beam milling experiments with *in situ* ion beam deposition, ion-assisted deposition, and planar triode sputtering, we have designed (in conjunction with L.M. Simard Co., Santa Barbara, CA) and purchased a multipurpose vacuum system with delivery anticipated in 1987. This unique ultra-high-vacuum system will allow for precision ion beam milling experiments with a fully articulating, cooled substrate fixture, as well as for a highly flexible array of thin film deposition and processing functions.

D. Waveguide Outcoupling Techniques

Another critical issue that must be addressed that is related to the area of waveguide design and fabrication is the development of a technique for uniform extraction of light from each waveguide in a direction normal to the surface of the integrated optics substrate. A number of potential methods are worthy of further investigation, including:

1. Uniform Overlayer

This is the most straightforward method for generating uniform leakage along a given waveguide. In this case, a thin film overlayer is chosen to have a specific refractive index that results in a very low loss per unit length from evanescent wave coupling. If the total waveguide loss is set to 5%, for example, then an essentially uniform vertical light leakage will result. This mode of operation is inefficient in its utilization of light from the laser diode source, however, since 95% of the light will be emitted from the far end of each waveguide and hence will not contribute to the detected intensity.

2. Nonuniform Overlayer

If the refractive index of the waveguide overlayer is varied along the length of the waveguide, the loss per unit length can be increased to make more efficient utilization of the incident illumination. The advantage of this method is the gain in overall throughput efficiency, but potential disadvantages are the complication of achieving a specific refractive index profile (or equivalently, a thickness profile of the overlayer) that allows uniform light loss per unit length, and the difficulty of generating sufficient refractive index variation or uniformity of thickness control to achieve the desired effect. A further inefficiency that complicates the uniform overlayer and nonuniform overlayer methods is the isotropic emission into a full hemisphere of the evanescently coupled light loss

from the layer, which places strict demands on the proximity coupling of the mask and photodetector required to capture a significant fraction of the emitted light.

3. Uniform Grating

A potential avenue of inquiry that circumvents a number of the limitations of the above two methods involves the corrugation of each waveguide along its length to produce a longitudinal grating coupler, as shown in Fig. 3. In this case, light will be emitted from the waveguide at the Bragg angle due to periodic coherent superposition effects. This allows for significantly enhanced latitude in detector proximity coupling, and can be fabricated with high uniformity. If the modulation depth of the corrugation is fixed as shown in Fig. 3, the modulation depth must be kept small to maintain a uniform incident intensity down the length of the waveguide.

In our initial experiments with grating outcoupling, we have utilized direct spin-coating of photoresist on top of slab waveguides in LiNbO_3 to produce an optically sensitive outcoupling layer. Gratings were holographically written in the photoresist layer by means of a specially designed interferometer illuminated by a He-Cd laser (441.6 nm). Grating periods of $1.4 \mu\text{m}$ were produced routinely in this arrangement.

Successful grating outcoupling was obtained over large areas ($4 \times 6 \text{ mm}$) with this technique. On the other hand, processing parameters required for obtaining high quality outcoupling proved extremely difficult to stabilize. This is principally due to the tradeoff between the modulation depth of the grating (which must be low to afford low efficiency but uniform coupling down the entire length of the waveguide) and the thickness of the photoresist in the grating valleys (which must be non-zero to promote non-negligible evanescent wave outcoupling, but not so thick as to exponentially attenuate the evanescent wave amplitude at the air-photoresist interface). In the follow-on program, we will explore ion milling of the grating directly into the waveguide surface as a means of producing a more reliable grating outcoupling process.

4. Nonuniform Grating

Perhaps the most promising technique of all involves alteration of the grating modulation depth along the length of the waveguide to allow a greater fraction of the light to be coupled out per unit length (compensating for the decreased intensity at each point in the waveguide with correspondingly increased modulation depth). Such a configuration is shown schematically in Fig. 4. This type of modulated corrugation could be produced by holographic interferometry within a photoresist layer, with longitudinal variation provided by space-variant reference and signal beam ratios. The photoresist pattern that results would then be subjected to ion beam milling to modulate the thickness of the rib waveguide.

WAVEGUIDE OUTCOUPLING : UNIFORM GRATING

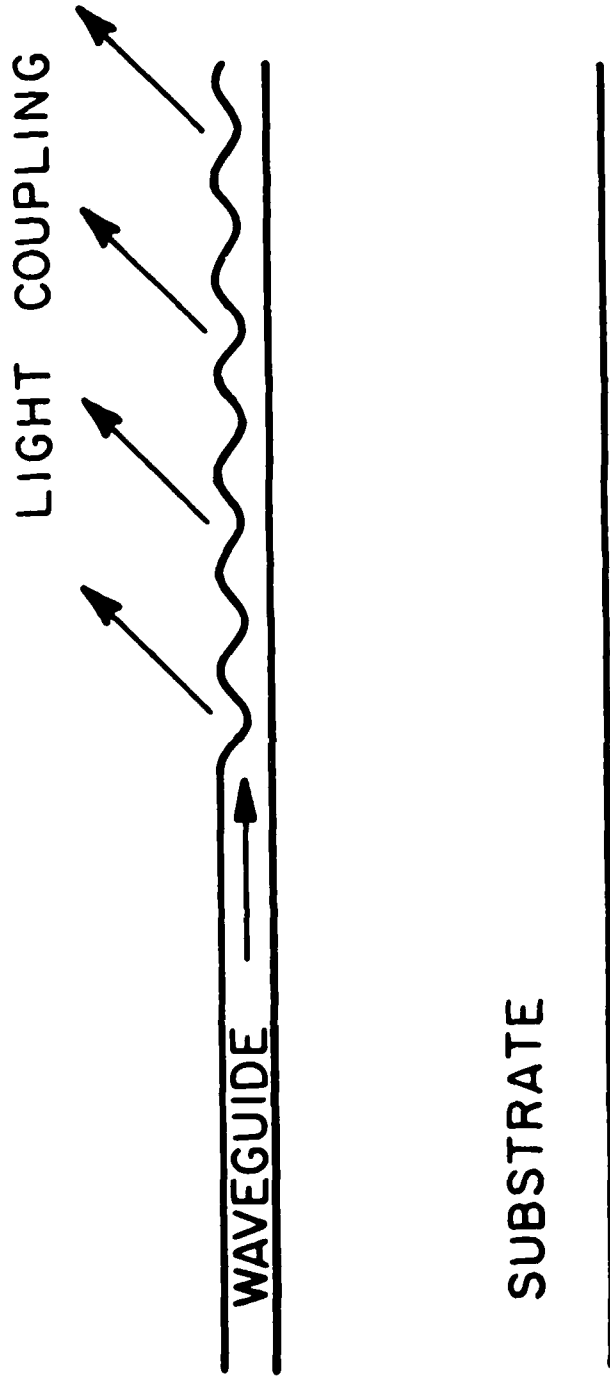


Fig. 3 Waveguide outcoupling from a rib or channel waveguide by uniform periodic modulation of the waveguide surface.

WAVEGUIDE OUTCOUPLING: NONUNIFORM GRATING

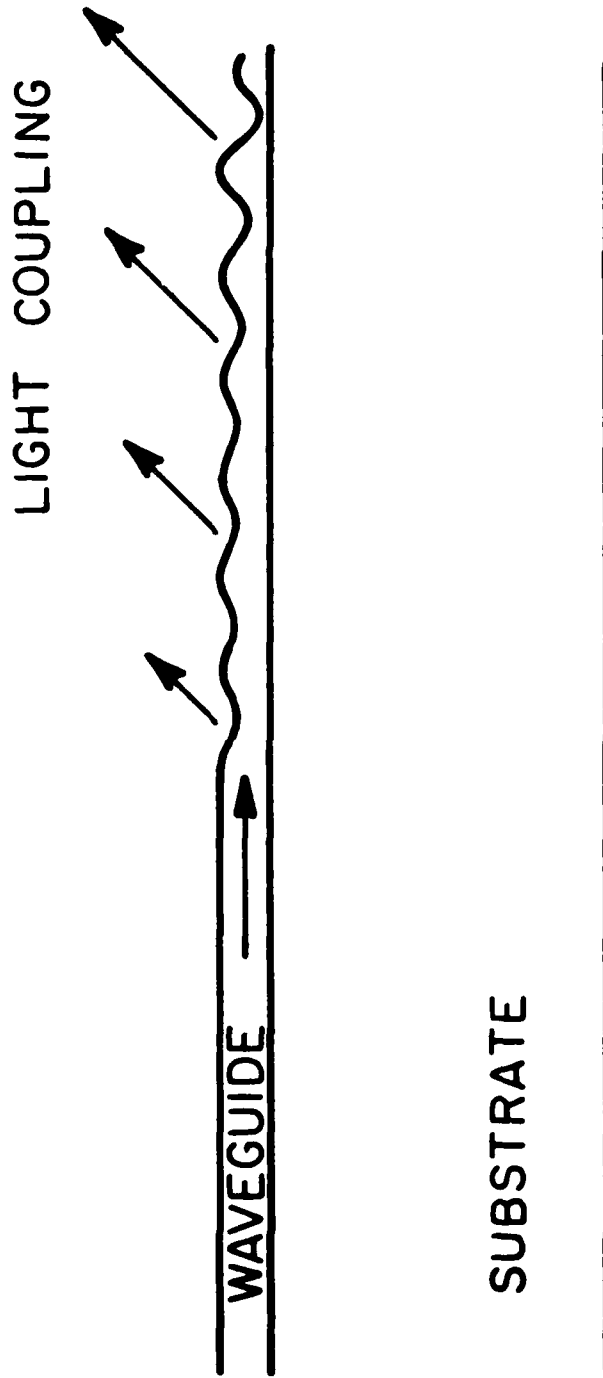


Fig. 4 Waveguide outcoupling from a rib or channel waveguide by nonuniform periodic modulation of the waveguide surface to compensate for outcoupling loss in the direction of propagation.

E. Incorporation of the Reference Beam

As described in Appendices A and B, a reference beam must be incorporated within the SAR processor architecture to re-encode the azimuth phase history (doppler-shift) as an amplitude modulation suitable for detection by the CCD array. During the contract period, we explored several potential methods for incorporation of the reference beam. The most straightforward of these is simply to add an appropriate frequency RF carrier to the SAR return signal, which will produce a reference beam appropriately doppler shifted from the laser frequency so that it can interfere with each separate range-focused beam at the entrance of the parallel rib waveguide array. This interference will produce the requisite amplitude modulation along the entire length of the array provided only that the coherence length of the pulsed laser is of order the length of the array.

F. CCD Detector Interface

Charge-coupled device arrays with adequate performance characteristics are commercially available at the present time. The electronic subsystem necessary to convert a commercial CCD array (designed as a closed-circuit TV camera) so that it can operate in the shift-and-add mode required by the SAR processor configuration described herein is similar in nature to an existing design fabricated previously at Caltech. The key issue here is the interface of the CCD to the integrated optical chip. Normally, a detector array is butt-coupled at one end of an integrated optical chip (and is usually a one-dimensional detector). In the proposed processor configuration we must couple the light out from the top of the integrated optical waveguides and onto a two-dimensional detector. There are (at least) two possible techniques for accomplishing this. The first is by means of proximity coupling. In this method, the mask and CCD combination are placed as close as possible to the surface of the integrated optical rib waveguide structure. The CCD cannot be placed in actual contact with the IO chip because the electrode structure of the CCD array would be potentially damaged, and in addition, the characteristics of the optical waveguides might be affected. One possible method by which this type of coupling could be effected is the application of a very thin (less than 50 micron) adhesive layer between the CCD array and the integrated optical chip. This layer must be nonconductive, optically transparent, and of index of refraction lower than that of either the IO substrate or the thin film overlayer (if such a layer is employed). Alternatively, the requisite light coupling can be accomplished by means of a thin air gap produced by microspacers.

G. Comparison with Present and Future Electronic Technology

In order to carefully assess the potential computational throughput gain, as well as the potential weight, power, and cost advantages of the IOSAR processor, we also initiated

during the contract period a direct comparison between current (and projected) electronic processors capable of synthetic aperture radar image formation and the projected performance of a fully functional (but not technologically advanced) IOSAR processor architecture. This study began by formulating the SAR image formation problem optimally for the IBM PC-XT with 8087 math co-processor chip as well as for the VAX-VMS 11/750 host. Preliminary results indicate a tremendous gain in overall computational throughput per unit power for the IOSAR architecture. These results will be further documented in the Final Report for the follow-on contract period. The comparative study has also included consideration of the possibility of using architecture mapping algorithms to map the SAR image formation problem onto a single VSLI or WSI chip. These efforts have not met with success, due primarily to the heavy interconnection burden required by the image formation algorithms.

H. Extensions of the Concept

The Integrated Optical Synthetic Aperture Radar Processor described in this proposal was conceived specifically for the SAR application. However, we believe that the novel concepts that we have discussed herein will have a much broader significance. The proposed configuration provides for the processing of inherently two-dimensional information in a planar integrated optical architecture. The information is processed in both the transverse and longitudinal dimensions of the integrated optical chip, and detected through utilization of the third dimension normal to the plane. This innovation, coupled with the time-and-space integration algorithm, allows extremely complicated two-dimensional operations to be performed at very high potential frame rates. There are several possible variations and extensions of this concept, as well as other problems to which it is clearly applicable.

First, methods for implementing a programmable IOSAR processor are of interest. In the particular implementation drawn schematically in Fig. 2, the azimuth reference is recorded on a fixed mask, and thus cannot be reprogrammed conveniently for SAR applications involving mobile platform geometries and dynamic reference conditions. One such method is the replacement of the fixed mask with a two-dimensional spatial light modulator that is electronically programmable to reflect the dynamic flight conditions requiring compensation.

Second, the direct implementation of other two-dimensional optical processing operations can be achieved utilizing the IOSARP configuration (with modifications in some cases). It is possible to implement any separable, two-dimensional signal processing operation using this approach. For example, a Fourier transform IO processor for image-based inputs is conceivable. The implementation of non-separable operations such as

two-dimensional correlations are more difficult, but still quite feasible. In particular, non-separable functions may be implemented by means of multiple input channel IO processors modeled after the single-channel device described in this report.

5. PUBLICATIONS

5.1 Published Manuscripts (AFOSR Sponsorship)

1. A. R. Tanguay, Jr., D. Psaltis, and T. J. Bicknell, "An Integrated Optical Synthetic Aperture Radar Processor", in preparation for Applied Optics.

5.2 Conference Presentations (AFOSR Sponsorship)

1. A. R. Tanguay, Jr., "Functional Requirements for Optical Processing and Computing", ITT Corporation Symposium on Ultra-High Bandwidth Communications, SEL Laboratories, Stuttgart, Federal Republic of Germany, (1985); (Invited Paper).
2. A. R. Tanguay, Jr., "Optical Computing Components: Fundamental Issues", 1985 Annual Meeting of the Optical Society of America, Washington, D.C., (1985); (Invited Paper).
3. T. Bicknell, D. Psaltis, and A. R. Tanguay, Jr., "Integrated Optical Synthetic Aperture Radar Processor" 1985 Annual Meeting of the Optical Society of America, Washington, D.C., (1985); J. Opt. Soc. Am. A, 2(13), P8, (1985).

6. SCIENTIFIC PERSONNEL

The following scientific personnel contributed to the research summarized in this report, and were either supported in part by the Air Force Office of Scientific Research or were supported in part by the University of Southern California through cost-sharing.

1. Professor Armand R. Tanguay, Jr., Principal Investigator
2. Kasra Rastani, Graduate Research Assistant
3. Bruce Damer, Graduate Research Assistant
4. Zaheed Karim, Graduate Research Assistant
5. Frank Lum, Senior Research Technician

7. REFERENCES

1. D. Psaltis and K. Wagner, "Real-Time Synthetic Aperture Radar (SAR) Processor", *Opt. Eng.*, 21, 822-828, (1982).
2. D. Psaltis, M. Haney, and K. Wagner, "Real Time Synthetic Aperture Radar Processing", *Proc. NASA Conference on Optical Information Processing for Aerospace Applications. II*, Langley, Virginia, (1983).
3. I. Abramov, Y. Owechko, A. R. Tanguay, Jr., and T. J. Bicknell, "Real Time Synthetic Aperture Image Formation Utilizing an Electrooptic Spatial Light Modulator", *Proc. NASA Spaceborne Imaging Radar Symposium, Jet Propulsion Laboratory Publication No. 83-11*, (1983).
4. B. A. Horwitz and F. J. Corbett, "The PROM-Theory and Applications for the Pockels Readout Optical Modulator", *Opt. Eng.*, 17, 353-364, (1978).
5. R. V. Johnson, D. L. Hecht, R. A. Sprague, L. N. Flores, D. L. Steinmetz, and W. D. Turner, "Characteristics of the Linear Array Total Internal Reflection (TIR) Electrooptic Spatial Light Modulator for Optical Information Processing", *Opt. Eng.*, 22, 665-674, (1983).
6. T. J. Bicknell, Jet Propulsion Laboratory, California Institute of Technology, private communication. See also D. A. Ausherman, "Digital versus Optical Techniques in Synthetic Aperture Radar (SAR) Data Processing", *Opt. Eng.*, 19, 157-167, (1980).
7. C. M. Verber, "Integrated Optical Approaches to Signal and Data Processing", *Proc. National Aerospace and Electronics Conference (NAECON 84)*, Dayton, Ohio, May, (1984).
8. C. M. Verber, R. P. Kenan, and J. R. Busch, "Correlator Based on an Integrated Optical Spatial Light Modulator", *Appl. Opt.*, 20, 1626-1629, (1981).
9. L. Thylen and L. Stensland, "Electrooptic Approach to an Integrated Optics Spectrum Analyzer", *Appl. Opt.*, 20, 1825-1832, (1981).
10. D. Psaltis, "Two Dimensional Optical Processing Using One Dimensional Input Transducers", *Proc. IEEE*, July, (1984), in press.
11. R. L. Holman and P. J. Cressman, "Optical Damage Resistance of Lithium Niobate Waveguides", *Opt. Eng.*, 21, 1025-1032, (1982).

12. D. Y. Zang and C. S. Tsai, "Single-Mode Waveguide Microlenses and Microlens Arrays Fabrication in LiNbO_3 Using Titanium Indiffused Proton Exchange Technique", Appl. Phys. Lett. 46(8), 703-705, (1985).

Real-time optical synthetic aperture radar (SAR) processor

Demetri Psaltis
Kelvin Wagner

California Institute of Technology
Department of Electrical Engineering
Pasadena, California 91125

Abstract. A real-time optical synthetic aperture radar (SAR) processor is described. The processor utilizes an acousto-optic device as the input electronic-to-optical transducer and a CCD camera that serves as the optical detector and simultaneously performs the focusing of the SAR image in the azimuth direction.

Keywords: two-dimensional signal processing; synthetic aperture radar; acousto-optic devices; imaging; image processing.

Optical Engineering 21(5), 822-828 (September/October 1982).

CONTENTS

1. Introduction
2. Synthetic aperture radar (SAR) signals
3. Acousto-optic/ CCD SAR processor
4. Discussion
 - 4.1. Azimuth resolution
 - 4.2. Image size in azimuth
 - 4.3. Range resolution
 - 4.4. Image size in range
 - 4.5. Flexibility
 - 4.6. Dynamic range
5. Experiment
6. Acknowledgments
7. Appendix A: derivation of Eq. (14)
8. Appendix B: derivation of Eq. (15)
9. References

1. INTRODUCTION

Synthetic aperture radar (SAR) still represents the most successful application of optical computing, even though more than 30 years have elapsed since the initial demonstration of the optical SAR processor. Optical computers are used routinely today to form SAR images from radar signals that are collected by aircraft or spacecraft and recorded on photographic film. The requirements of modern radars, however, are often not met by the present film-based optical processors. These requirements include higher image quality (resolution, dynamic range, artifacts, etc.), real-time image formation, flexibility, and on-board processing capability. In order to meet such requirements, digital computers are increasingly being used to form SAR images. The dramatic advances in microelectronics in recent years have made it feasible to construct digital SAR processors that can provide better image quality (due to the highest accuracy and the flexibility in programming a digital computer) than film-based SAR processors. In addition, digital processors can be built (as they have in some cases) that have real-time and on-board processing capabilities. It is not the purpose of this paper to present a comparison of optical versus digital techniques in SAR (the interested reader is referred to Ausherman's paper¹), but it is necessary to point out that a number of problems remain with digital SAR processors. The complexity of these systems results in a very costly, power consuming, relatively large

and heavy processor. Thus, even though it is conceivable to build a low resolution real-time digital processor, for many of the applications this is an impractical solution.

Very significant advances have also been achieved in the area of electro-optics which have resulted in corresponding improvements in the state of the art of optical computers. Specifically, acousto-optic technology has matured, and consequently high quality devices are now available to be used as the input spatial light modulator; semiconductor detector arrays (CCD's and photodiode arrays) have proven to be excellent as detectors in the optical computer, and the semiconductor light sources (LED's and laser diodes) which have been developed primarily for optical communications, are a very efficient light source in many optical processors. These and other developments have made it possible to construct real-time, high performance, power efficient, compact and relatively inexpensive optical computers such as the acousto-optic spectrum analyzer² and the ambiguity function radar processors.³ In this paper we describe an optical SAR processor in which the modern components available for optical computing are fully utilized, and, therefore, we believe that the resulting processor has great potential for applications where on-board, real-time SAR image formation is required.

In Sec. 2 the fundamentals of SAR are reviewed, in order to establish the notation we will be using in the paper. A comprehensive treatment of SAR can be found in Refs. 4 and 5. In Sec. 3 the operation of the optical processor is described in detail, and in Sec. 4 we discuss its performance characteristics. Our experimental results to date are reported in Sec. 5.

2. SAR SIGNALS

The side-looking SAR geometry is depicted in Fig. 1. The vehicle (aircraft or spacecraft) is traveling with a constant velocity v along the η direction and at height h . Coded pulses are emitted periodically through an antenna mounted on the side of the vehicle. In this paper we assume that the pulses are chirp coded. The transmitted waveforms $S(t)$ in complex notation is given by

$$S(t) = \sum_n \text{rect} \left[\frac{t-nT}{\tau} \right] \exp[jb(t-nT)^2] \exp(j2\pi\nu_0 t), \quad (1)$$

where τ is the pulse duration, $1/T$ is the pulse repetition frequency (PRF), b is the chirp rate, and ν_0 is the microwave frequency of the radar. The transmitted waveform illuminates a patch of the surface to be imaged (the ground), and part of it is reflected back towards the

Invited Paper TD-103 received Apr. 12, 1982, accepted for publication Apr. 19, 1982, received by Managing Editor May 10, 1982.
© 1982 Society of Photo-Optical Instrumentation Engineers.

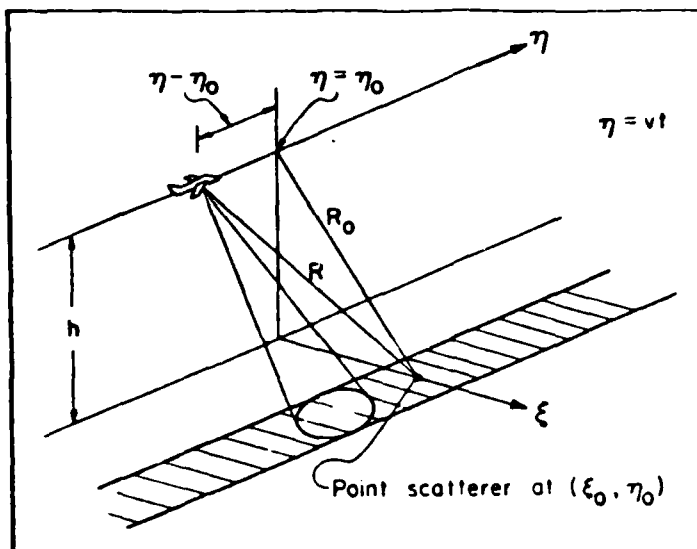


Fig. 1. Synthetic aperture radar geometry.

vehicle and detected by the antenna. The objective of SAR is to form an image of the ground from these reflections. We will discuss how an image of a single point scatterer (impulse) located at coordinates $\xi = \xi_0$ and $\eta = \eta_0$ on the ground can be formed. Since the SAR image formation is a linear operation, knowledge of the impulse response completely describes the system. The signal received by the antenna due to a single point scatterer is

$$r(t) = A(t)S(t - 2R/c) \quad (2)$$

where R is the instantaneous range from the antenna to the point scatterer at (ξ_0, η_0) . $A(t)$ is the far-field pattern of the antenna. From the geometry of Fig. 1, R can be written as

$$R(t) = \sqrt{(\eta_0 - \eta)^2 + R_0^2} = \sqrt{(\eta_0 - vt)^2 + R_0^2} \quad (3)$$

where $R_0 = \sqrt{h^2 + \xi_0^2}$ is the range when the vehicle crosses $\eta = \eta_0$. In most cases, the variation of the range $R(t)$ with time can be neglected within the duration τ of a single radar pulse, and therefore $R(t) \approx R(nT)$. In addition, the range R_0 is typically much greater than the distance $|\eta - \eta_0|$. This allows us to expand the square root in Eq. (3) as follows:

$$R(t) \approx R(nT) = R_0 + \frac{(vnT - \eta_0)^2}{2R_0} \quad (4)$$

Using the above equation and Eq. (1), we can rewrite Eq. (2) as

$$r(t) = \sum_n A(nT) \text{rect} \left[\frac{t - 2R_0/c - \Delta r - nT}{\tau} \right] \times \exp[jb(t - 2R_0/c - \Delta r - nT)^2] \times \exp(j2\pi\nu_0 t) \exp(-j2\pi\nu_0 2R_0/c) \exp(-j2\pi\nu_0 \Delta r) \quad (5)$$

The variation of the antenna pattern $A(t)$ during a single pulse can be neglected, and hence $A(t) \approx A(nT)$. The quantity $\Delta r = (vnT - \eta_0)^2 / R_0$ has units of time and is very small compared to $2R_0/c$ if $R_0 \gg |\eta - \eta_0|$. Therefore, Δr can be neglected in Eq. (5) except in the term $\exp(-j2\pi\nu_0 \Delta r)$ because in this term Δr is multiplied by ν_0 which is the very large radio frequency. The term $\exp(-j4\pi\nu_0 R_0/c)$ is an inconsequential constant phase term and can be omitted. With these modifications, we can write the final form for $r(t)$ as

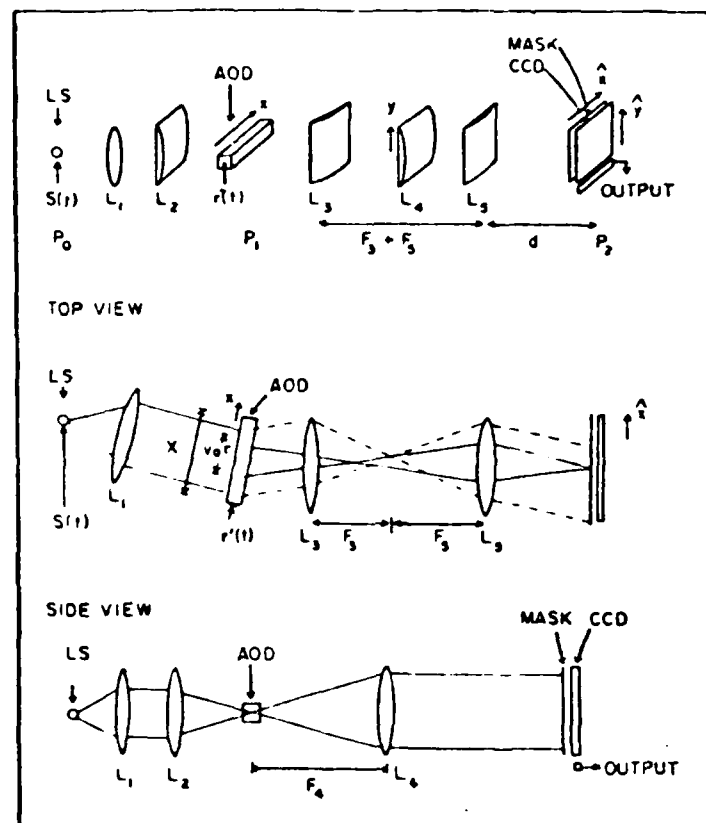


Fig. 2. Acousto-optic/CCD synthetic aperture radar processor. (LS—light source, AOD—acousto-optic device, F_i is the focal length of the lens L_i , and the broken lines indicate the path of the rays of the reference wave.)

$$r(t) = \sum_n A(nT) \text{rect} \left[\frac{t - 2R_0/c - nT}{\tau} \right] \times \exp[jb(t - 2R_0/c - nT)^2] \exp[-j(2\pi\nu_0/cR_0)(vnT - \eta_0)^2] \times \exp(j2\pi\nu_0 t) \quad (6)$$

The received signal $r(t)$ must be processed to produce an image of the point scatterer on the ground. In the next section we will describe in detail how the real-time optical processor that is presented in this paper forms the SAR image from the signal $r(t)$. In deriving Eq. (6), a number of simplifying assumptions and approximations were made, which may or may not be justifiable in practice depending on the particular application. We will proceed with the description of the system based on this relatively simple form of the SAR equation [Eq. (6)], and in Sec. 4 we will discuss the necessary modifications to the system for cases in which the conditions set in this section are not met.

3. ACOUSTO-OPTIC/CCD SAR PROCESSOR

A schematic diagram of the processor is shown in Fig. 2. The system is illuminated by a pulsed laser. The light amplitude of the source is modulated by

$$P(t) = \sum_n \text{rect} \left[\frac{t - nT}{\tau_0} \right] \quad (7)$$

where τ_0 is the duration of each light pulse. The spherical lens L_1 collimates the light from the source, and the cylindrical lens L_2 focuses the light in the vertical (y) direction so that it can pass through the aperture of the acousto-optic device (AOD) placed in plane P_1 . The received radar signal $r(t)$ is heterodyned to the center frequency ν_1 of the AOD, and a reference signal $B \exp(j2\pi\nu_2 t)$ is

added to it. The frequency ν_2 is chosen such that the difference $\nu_2 - \nu_1$ is equal to the bandwidth of each radar pulse:

$$\nu_2 - \nu_1 = br/\pi. \quad (8)$$

The need for the reference signal will become apparent shortly. The resulting signal $r'(t)$ is related to $r(t)$ by the following equation:

$$r'(t) = r(t) \exp[-j2\pi(\nu_2 - \nu_1)t] + B \exp(j2\pi\nu_2 t). \quad (9)$$

$r'(t)$ is applied to the piezoelectric transducer of the AOD of Fig. 2. The light diffracted by the AOD is modulated by⁶

$$S_1(t, x) = \text{rect} \left(\frac{x}{X} \right) P(t) r' \left(t + \frac{x}{v_a} \right). \quad (10)$$

where x is along the direction of propagation of the acoustic wave, X is the aperture of the AOD, and v_a is the speed of sound in the AOD. The undiffracted light is blocked in the focal plane of the cylindrical lens L_3 . The combination of lenses L_3 and L_4 accomplishes two tasks. First, since the two lenses are separated by the sum of their focal lengths, a single plane wave incident on L_3 will be recollimated when it exits the lens L_4 . In addition, the impulse response of the system in the x direction from plane P_1 to plane P_2 is made to be equal to

$$h(x, \bar{x}) = \exp[jb_1(x - \bar{x})^2] \exp(-j2\pi\nu_1 x/v_a). \quad (11)$$

where \bar{x} is the horizontal coordinate in plane P_2 . The constant b_1 can be set by appropriately choosing the focal lengths of L_3 and L_4 and the distance d . The term $\exp(-j2\pi\nu_1 x/v_a)$ reflects the fact that the optical system following the Bragg cell is tilted so that its optical axis coincides with a wave diffracted at the Bragg angle. In Eq. (11) we assume that the effects of the lens apertures are negligible. In the vertical direction y , the light is recollimated by the lens L_4 , and therefore the amplitude of light entering plane P_2 does not vary along y . At P_2 a transparency is placed immediately in front of the CCD camera. The intensity transmittance $T(\bar{x}, \bar{y})$ of this mask is

$$T(\bar{x}, \bar{y}) = \frac{1}{2} + \frac{1}{2} \cos \left[2\pi u_0 \bar{x} + \frac{b_2 \bar{y}^2}{\bar{x}} \right], \quad (12)$$

where u_0 and b_2 are constants that will be specified later. The instantaneous intensity incident on the CCD is given by

$$I(\bar{x}, \bar{y}, t) = T(\bar{x}, \bar{y}) \left| \int S_1(t, x) h(x, \bar{x}) dx \right|^2 \quad (13)$$

The CCD is operated in the shift-and-add mode.⁷ In this mode of operation the device is exposed to light periodically. The photogenerated charge is accumulated on the detector for a short time interval, and after each exposure the entire photogenerated charge pattern is electronically shifted by one pixel along one of the dimensions of the CCD. The photogenerated charge due to the next exposure is simply added to the charge that is already stored in each pixel, and then the process is repeated. In our system the charge transferring is done in synchronism with the PRF of the radar, and the integration period is set equal to the period T of the radar. The charge generated on the CCD during the n th radar pulse is given by

$$\begin{aligned} Q(\bar{x}, \bar{y}, n) &= \int_{t-nT/2}^{t+nT/2} I(\bar{x}, \bar{y}, t) dt \\ &= 2Bv_a r r_0 T(\bar{x}, \bar{y}) A(nT) \text{sinc} \left[\frac{br}{\pi v_a} \left(\bar{x} - \frac{2R_0 v_a}{c} \right) \right] \end{aligned}$$

$$\begin{aligned} &\times \cos \left[\frac{2\pi(\nu_2 - \nu_1)\bar{x}}{v_a} + \frac{2\pi\nu_0}{cR_0} (v_n T - \eta_0)^2 + \phi \right] \\ &+ \text{bias terms} \end{aligned} \quad (14)$$

The derivation of Eq. (14) is straightforward but tedious, and it is presented in Appendix A. This charge pattern gets shifted along the \bar{y} direction by $(N - n)$ pixels on the CCD, after N exposures have taken place. The total charge that accumulates at each pixel located at coordinates (\bar{x}, \bar{y}) after N exposures is

$$\begin{aligned} Q(\bar{x}, \bar{y}) &= \sum_n^N Q[\bar{x}, \bar{y} + (N - n)\Delta y, n] \\ &= \frac{Bv_a r r_0}{2} \text{sinc} \left[\frac{br}{\pi v_a} \left(\bar{x} - \frac{2R_0 v_a}{c} \right) \right] \text{sinc} \left[\frac{2Nv_0 v^2 T^2}{c\Delta y R_0} \right] \\ &\times \left(\bar{y} - \eta_0 \frac{\Delta y}{vT} + N\Delta y \right) \cos [4\pi u_0 \bar{x} + \phi] \\ &+ \text{bias terms}. \end{aligned} \quad (15)$$

In the above equation Δy is the pixel separation in the CCD, $u_0 = (\nu_2 - \nu_1)/v_a$, and ϕ is a constant phase term. $Q(\bar{x}, \bar{y})$ is the final output of the processor, and its form demonstrates the imaging capability of the system. In the \bar{x} direction, $Q(\bar{x}, \bar{y})$ is a sinc function with width $\pi v_a / br$ and centered at $\bar{x} = 2R_0 v_a / c$. In other words, we obtain the image of the point scatterer located at $\xi = \xi_0$ on the ground, focused in the ξ direction. The resolution in the ξ direction is equal to $\delta_\xi = \pi c / 2br$. This is a well-known result for range resolution in radar systems.⁸ The carrier at spatial frequency $2u_0$ arises from the inclusion of the reference signal in the acousto-optic device which allowed us to record on the CCD the phase of the detected signals. This is necessary in this system because the Doppler information that is essential for the focusing in the azimuth (η) direction is encoded in the phase of the range compressed signal $Q(\bar{x}, \bar{y}, n)$. In addition, since the output forms on a carrier, it can be easily separated from the bias term in Eq. (15).

In the \bar{y} direction, $Q(\bar{x}, \bar{y})$ is also a sinc function whose position is proportional to η_0 , the location of the point scatterer on the ground in the azimuth direction. The width of this sinc function is equal to $c\Delta y R_0 / Nv_0 v^2 T^2$, and it determines the resolution in azimuth. In ground coordinates η , the width of the sinc function corresponds to an azimuth resolution

$$\delta_\eta = \frac{cR_0}{2Nv_0 vT} = \lambda_0 R_0 / 2D_s.$$

$D_s = NvT$ is the distance that the vehicle collecting the SAR data travels during the time interval NT , and it is equal to the synthetic aperture of the system. Therefore, the azimuth resolution obtained with this processor conforms with previously derived results⁹ for SAR systems. The entire pattern is shifted in the \bar{y} dimension by the distance $N\Delta y$. For a CCD with N pixels in the horizontal direction, this implies that after the signal is integrated on the CCD for N pulses to produce a focused image, it arrives at the edge of the device (at $\bar{y} = N\Delta y$) where a separate CCD stage transfers an entire line of the data (a slice of the image for each azimuth position) to the output pin of the CCD device. The azimuth slices are continuously produced as long as the flight continues, producing in real time an image of a long strip on the ground parallel to the direction of the flight.

4. DISCUSSION

In this section we discuss some of the issues relative to the performance of the optical processor we have described. We will address

several performance criteria separately and comment on the effects of the processor architecture and the devices used in the system. A complete in-depth analysis of the performance is beyond the scope of this paper.

4.1. Azimuth resolution

In the previous section we derived the formula for the resolution that can be obtained in the along track (azimuth) direction.

$$\delta_{\eta} = \frac{cR_0}{2Nv_0T} \quad (16)$$

N is the only parameter in the above equation that is related to the processor. N is the number of radar pulses that are used to form the SAR image of each point scatterer on the ground. In the AO/CCD processor, N is also equal to the number of pixels of the CCD in the shifting direction (\hat{y}). Commercially available CCD cameras have approximately 500 pixels. Several devices with approximately twice this number have recently been developed⁸ or are currently under development. If a CCD with 10^3 pixels is used, the azimuth resolution obtainable with this processor is 22.5 meters on the ground. This figure was obtained by using the parameters of the SEASAT radar⁹ that was flown by NASA. The azimuth resolution will, of course, be different for different radars. To obtain lower resolution, larger CCD's would have to be used. It is unlikely that a significant increase in the size of monolithic CCD cameras will take place in the near future. It is possible, however, to construct larger arrays by interfacing a number of separate chips. As N is increased and finer resolution is achieved, other factors in the processor become limiting, such as optical aberrations, mechanical/electronic stability, and light source coherence over the time period NT . Finally, for low resolution imaging, some of the approximations that were made in Sec. 2 may not be valid. For instance, if the approximation that the range of each point target remains constant as the plane flies past it is not valid, an effect known as range curvature⁴ results. Range curvature can be corrected in our processor simply by tilting one of the cylindrical lenses in the system which introduces barrel distortion that can exactly cancel out the range curvature.

4.2. Image size in azimuth

The AO/CCD processor continuously produces slices of the SAR images in the azimuth direction, and therefore the size of the SAR image is not limited by the processor in this direction.

4.3. Range resolution

The resolution in the range direction (ξ) on the ground is given by

$$\delta_{\xi} = \frac{\pi c}{2b_T} \quad (17)$$

The bandwidth of the chirped radar pulses is equal to b_T/π , and therefore the resolution in range is limited by the temporal bandwidth of the processor. The bandwidth of the AOD used in the system is not the primarily limiting factor since devices with several gigahertz bandwidth are available. More importantly, the duration of the light pulse τ_0 must be shorter than the inverse of the bandwidth of the signal to avoid smearing of the range compressed signal [Eq. (14)]. For typical radar bandwidths, τ_0 should be several nanoseconds. Several laser sources are capable of producing nanosecond pulses with adequate peak power. We are primarily considering laser diodes because they are compact and power efficient. Laser diodes can lase in a single mode under cw operation (and therefore be coherent), but when they are pulsed, several modes exhibit gain during the transients. The need for coherence in the system imposes with present state-of-the-art devices a minimum pulse width of ~ 20 ns. Therefore, if a laser diode is used in the system, the bandwidth of the radar must be equal to 50 MHz, which corresponds to range resolution equal to 3 m. This can be lowered by an order of magni-

tude if a pulsed gas laser is used. The additional factors mentioned in our discussion on azimuth resolution also become increasingly important for finer range resolution.

4.4. Image size in range

The number of pixels in the range direction is limited by the space-bandwidth product of the AOD or the CCD in the nonshifting direction, whichever is smaller. At the present time, the CCD imposes this limit at approximately 10^3 pixels. The range coverage can be extended by using several processors operating in parallel.

4.5. Flexibility

A potential application for the AO/CCD processor is on-board real-time image formation. In such applications the radar geometry can be expected to change from time to time or even continuously. Enough flexibility must be built into the system so that it can be adaptable to the changing conditions. One method for achieving this is by the use of a real-time 2-D spatial light modulator⁶ in place of the fixed mask in Fig. 2. The impulse response of the processor can then be altered to track changes in the radar geometry.

4.6. Dynamic range

The dynamic range is defined as the maximum unsaturated brightness in the SAR image divided by the minimum detectable level above the noise. In general, a large dynamic range can be observed in a SAR image because the noise detected at radio frequencies is very effectively suppressed through the pulse compression in both range and azimuth that is performed to bring the SAR image into focus. The potential for high dynamic range, however, can only be realized if the processor that forms the SAR image can provide it. In an optical processor, essentially every component of the system contributes to diminish the dynamic range available at the output by adding noise or by introducing nonlinearities and aberrations in the system. In the AO/CCD processor, the CCD detector is the dominant factor that limits the dynamic range. The maximum brightness of the SAR image is equal to the maximum charge that can be stored in each pixel of the CCD, minus the charge that corresponds to the bias terms in Eq. (15) and the dark current that accumulates during the integration time. The bias is signal dependent and is largest at portions of the SAR image that have maximum average intensity. Therefore, relatively sparse objects can be imaged with a larger dynamic range. For a single point scatterer on the ground, the bias can be only 1/2 of the full dynamic range of the CCD, but for a distributed target the bias increases as \sqrt{M} , where M is the average number of point scatterers on the ground that are located at the same range in a distance NvT along the azimuth direction. The minimum detectable level at the output of the processor is determined by the fixed pattern noise of the CCD (the variation of the dark current from pixel to pixel), optical scattering, quantum noise primarily due to the bias, and thermal and amplifier noise from the electronics.¹⁰ Our calculations¹¹ show that the dynamic range of the images that will be produced by the experimental processor we are presently constructing is $\sim 200:1$. A commercially available CCD camera is used in the experimental processor, and post-detection signal processing is applied in order to minimize noise. The dynamic range can be increased to over $10^3:1$ by cooling the CCD to eliminate the dark current and by using a CCD specifically designed for this application.

5. EXPERIMENT

The CCD camera is utilized in this system not only as the optical detector but also as a multichannel correlator by operating it in the shift-and-add mode described earlier. The signal that comes out at each column (at position \bar{x}) of the device is the correlation between the transmittance of the mask as a function of \bar{y} at the same position \bar{x} and the signal corresponding to the temporal variation of the incident light intensity. We have performed an experiment to demonstrate the operation of the CCD as an optical multichannel correlator. The experimental setup is shown in Fig. 3. A light emitting diode (LED) is used as the light source. The intensity of the LED is

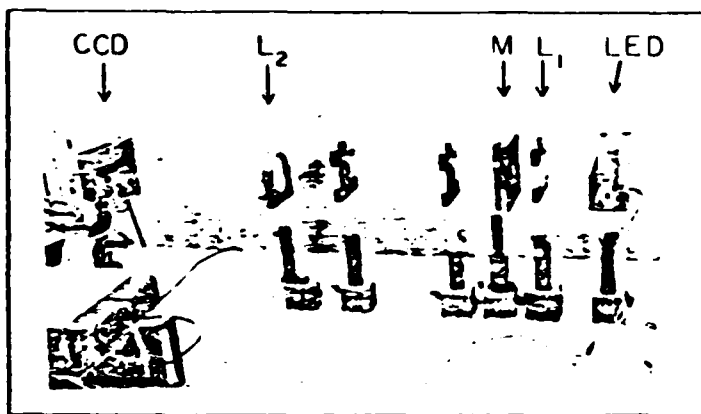


Fig. 3. Experimental electro-optic ambiguity function processor. (LED—light emitting diode, L_1 —collimating lens, M —mask, L_2 —imaging lens, CCD—camera.)

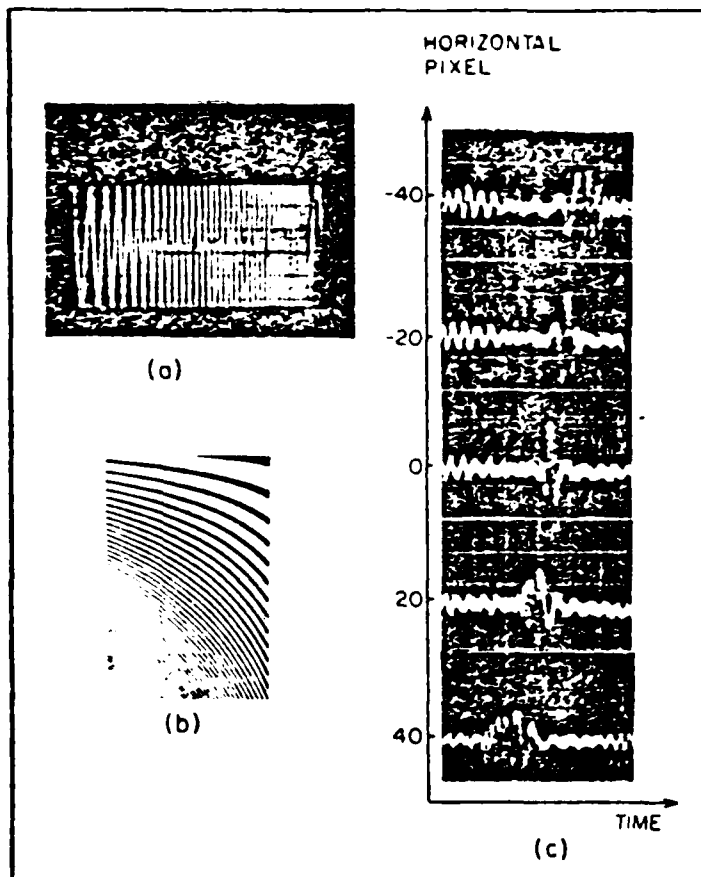


Fig. 4. Ambiguity processor signals: (a) input (LED) waveform; (b) mask; (c) ambiguity function.

temporally modulated by the chirp signal shown in Fig. 4(a). The chirp signal that modulates the LED represents the variation of the intensity detected by the CCD [the function $Q(\hat{x}, \hat{y}, n)$ in Eq. (14)] as a function of pulse number n . The duration of this waveform is equal to NT , and its bandwidth is equal to $v_o v^2 NT / cR_o$. The bandwidth of the waveform in Fig. 4(a) is 30 Hz, and its duration is 1 s. The CCD we used in this experiment has $N = 512$ pixels in the vertical dimension, and therefore the duration of one second corresponds to a radar pulse repetition frequency equal to $1/T = 0.5$ kHz. These parameters were chosen to be approximately equal to the parameters of an experimental aircraft radar which is flown periodically by the Jet Propulsion Laboratory. We intend to use data collected by this radar to test the processor when it is completed.

The light from the LED is collimated by lens L_1 in Fig. 3, and it

illuminates the mask denoted by M in Fig. 3. A photograph of this mask is shown in Fig. 4(b). The intensity transmittance in the vertical direction is a chirp signal whose chirp rate is proportional to the horizontal position. The signal at the center of the mask matches the waveform that is used to modulate the LED. The mask is imaged by lens L_2 onto the CCD, which is operated in the shift-and-add mode. The output signal from the CCD at each horizontal position is the correlation of the waveform modulating the LED and the transmittance of the mask at that horizontal position. The output waveforms from the CCD from selected vertical locations are shown in Fig. 4(c). This 2-D waveform is known as the ambiguity function¹² of the chirp signal, and Fig. 4(c) displays the familiar tilted-ridge structure of the ambiguity function for this particular waveform.

6. ACKNOWLEDGMENTS

We thank Tom Bicknell from the Jet Propulsion Laboratory (JPL) for the technical information he has provided to us on SAR systems and for loaning to us some of the equipment used in the experiments. The research reported in this paper is supported by NASA and JPL and in part by the Air Force Office of Scientific Research.

7. APPENDIX A: DERIVATION OF EQUATION (14)

$$Q(\hat{x}, \hat{y}, n) = \int_{t-nT/2}^{t+nT/2} I(\hat{x}, \hat{y}, t) dt \quad (14)$$

Substituting Eq. (13) in Eq. (14):

$$Q(\hat{x}, \hat{y}, n) = T(\hat{x}, \hat{y}) \int_{t-nT/2}^{t+nT/2} \left| \int S_1(t, x) h(x, \hat{x}) dx \right|^2 dt \quad (A1)$$

We will first evaluate the integral over x in the above expression. Using Eqs. (10) and (11):

$$\begin{aligned} g(t, \hat{x}) &= \int S_1(t, x) h(x, \hat{x}) dx \\ &= \int \text{rect} \left(\frac{x}{X} \right) P(t) r' \left(t + \frac{x}{v_a} \right) \exp[jb_1(x - \hat{x})^2] \\ &\quad \times \exp \left(-j \frac{2\pi v_1 x}{v_a} \right) dx \quad (A2) \end{aligned}$$

Substituting the expressions for $P(t)$ and $r'(t)$ from Eqs. (7) and (9):

$$\begin{aligned} g(t, \hat{x}) &= \sum_n \text{rect} \left(\frac{t-nT}{T} \right) \int \text{rect} \left(\frac{x}{X} \right) \\ &\quad \times \left\{ r \left(t + \frac{x}{v_a} \right) \exp \left[-j2\pi(v_o - v_1) \left(t + \frac{x}{v_a} \right) \right] \right. \\ &\quad \left. + B \exp \left[j2\pi v_2 \left(t + \frac{x}{v_a} \right) \right] \right\} \\ &\quad \times \exp[jb_1(x - \hat{x})^2] \exp \left(\frac{-j2\pi v_1 x}{v_a} \right) dx \quad (A3) \end{aligned}$$

and the expression for the received signal $r(t)$ from Eq (6) is

$$\begin{aligned}
 g(t, \hat{x}) = & \sum_n \text{rect} \left(\frac{t-nT}{\tau_0} \right) \int \text{rect} \left(\frac{x}{X} \right) \left\{ \sum_n A(nT) \text{rect} \left[\frac{t-2R_0 c - nT + x v_a}{\tau} \right] \exp [j b (t - 2R_0 c - nT + x v_a)^2] \right. \\
 & \times \exp \left[-j \frac{2\pi v_0}{c R_0} (v_n T - \eta_0)^2 \right] \exp [j 2\pi v_0 (t + x v_a)] \exp [-j 2\pi (v_2 - v_1) (t + x v_a)] + \text{Bexp} [j 2\pi v_2 (t + x/v_a)^2] \left. \right\} \\
 & \times \exp [j b_1 (x - \hat{x})^2] \exp (-j 2\pi v_1 x/v_a) dx \quad (A4)
 \end{aligned}$$

The laser pulse width τ_0 is chosen sufficiently smaller than the bandwidth of the radar pulses ($\tau_0 < b r / \pi$) so that the temporal variation of the signal in the above equation can be neglected over the duration of each light pulse. With this approximation Eq (A4) can be rewritten as follows.

$$\begin{aligned}
 g(t, \hat{x}) = & \sum_n \text{rect} \left(\frac{t-nT}{\tau_0} \right) \exp (j 2\pi v_1 t) \int \text{rect} \left(\frac{x}{X} \right) \left\{ \sum_n A(nT) \text{rect} \left[\frac{x v_a - 2R_0 c}{\tau} \right] \exp [j b (x v_a - 2R_0 c)^2] \right. \\
 & \times \exp \left[\frac{-j 2\pi v_0}{c R_0} (v_n T - \eta_0)^2 \right] + \text{Bexp} [j 2\pi (v_2 - v_1) x v_a] \exp [j 2\pi (v_2 - v_1) nT] \left. \right\} \exp [j b_1 (x - \hat{x})^2] dx \quad (A5)
 \end{aligned}$$

We can assume that $|X| > v_a \tau + 2R_0 v_a/c$, i.e., the range delay is such that the reflected radar pulse is entirely in the aperture of the AOD at the instant the laser is pulsed. This can be ensured by appropriately setting the relative phase of the radar and laser pulse repetition frequencies. The parameter b_1 (the focusing power of the optical system in the x direction) is set equal to b/v_a^2 . Finally, the offset frequency $v_2 - v_1$ is made to be equal to m/T , where m is an integer. This can be accomplished by deriving $v_1 - v_2$ from the pulse repetition frequency $1/T$. The function $g(\hat{x}, t)$ can then be written as follows:

$$\begin{aligned}
 g(\hat{x}, t) = & \sum_n \text{rect} \left(\frac{t-nT}{\tau_0} \right) \left\{ A(nT) \exp \left[-j \frac{2\pi v_0}{c R_0} (v_n T - \eta_0)^2 \right] \exp \left(-j \frac{b}{v_a^2} \hat{x}^2 \right) \exp \left(j \frac{4b R_0^2}{c^2} \right) \int \text{rect} \left(\frac{x/v_a - 2R_0/c}{\tau} \right) \right. \\
 & \times \exp \left[-j \frac{2b}{v_a^2} (\hat{x} - 2R_0 v_a/c) x \right] dx + \text{Bexp} [j 2\pi (v_2 - v_1) \hat{x}/v_a] \exp [j \pi^2 (v_2 - v_1)^2/b] \left. \right\} = \sum_n \text{rect} \left(\frac{t-nT}{\tau_0} \right) \\
 & \times \left\{ A(nT) v_a \tau \text{sinc} \left[\frac{b r}{\pi v_a} (\hat{x} - 2R_0 v_a/c) \right] \exp \left[-j \frac{2\pi v_0}{c R_0} (v_n T - \eta_0)^2 \right] \exp \left[-j \frac{2b}{v_a^2} (\hat{x} - 2R_0 v_a/c) (2R_0 v_a/c) \right] \right. \\
 & \times \exp \left[-j \frac{b}{v_a^2} (\hat{x}^2 - 4R_0^2 v_a^2/c^2) \right] + \text{Bexp} [j 2\pi (v_1 - v_2) \hat{x}/v_a] \exp [j \pi^2 (v_2 - v_1)^2/b] \left. \right\} \quad (A6)
 \end{aligned}$$

We substitute the above expression in Eq. (14):

$$\begin{aligned}
 I(\hat{x}, \hat{y}, nT) = & T(\hat{x}, \hat{y}) \int_{t-nT-2}^{t+nT+2} \sum_n \text{rect} \left(\frac{t-nT}{\tau_0} \right) \left\{ |A(nT)|^2 v_a^2 \tau^2 \text{sinc}^2 \left[\frac{2b r}{v_a} (\hat{x} - 2R_0 v_a/c) \right] + |B|^2 + 2B A(nT) v_a \right. \\
 & \times \text{sinc} \left[\frac{b r}{\pi v_a} (\hat{x} - 2R_0 v_a/c) \right] \cos \left[\frac{2\pi (v_2 - v_1) \hat{x}}{v_a} + \frac{2\pi v_0}{c R_0} (v_n T - \eta_0)^2 + \phi \right] \left. \right\} dt = 2T(\hat{x}, \hat{y}) B v_a \tau_0 A(nT) \\
 & \times \text{sinc} \left[\frac{b r}{\pi v_a} (\hat{x} - 2R_0 v_a/c) \right] \cos [2\pi (v_2 - v_1) \hat{x}/v_a + 2\pi v_0 (v_n T - \eta_0)^2/c R_0 + \phi] + \text{bias terms} \quad (14)
 \end{aligned}$$

In the above equation, the phase terms from Eq. (A6) that do not depend on the index n have been lumped in the parameter ϕ .

8. APPENDIX B: DERIVATION OF EQUATION (15)

$$Q(\tilde{x}, \tilde{y}) = \sum_n^N Q(\tilde{x}, \tilde{y} - n\Delta y + N\Delta y, nT). \quad (15)$$

Substitute Eq. (14) in the above equation and the expression for the transmittance of the mask from Eq. (12):

$$\begin{aligned} Q(x, y) = & \sum_n^N 2Bv_o \tau r_o \left\{ \frac{1}{2} + \frac{1}{2} \right. \\ & \times \cos \left[2\pi u_o \tilde{x} - \pi b_2 (\tilde{y} - (n-N)\Delta y)^2 / \tilde{x} \right] \\ & \times A(nT) \operatorname{sinc} \left[\frac{br}{\pi v_o} (\tilde{x} - 2R_o v_o / c) \right] \\ & \left. \times \cos \left[2\pi (v_2 - v_1) \tilde{x} / v_o + 2\pi v_o (v_n T - \eta_o)^2 / c R_o + \phi \right] \right\}. \quad (B1) \end{aligned}$$

The spatial frequency u_o on the mask must be selected so that the sum frequency $u_o + (v_2 - v_1) / v_o$ of the two cosine functions in the above equation is sufficiently large so that the signal term that is riding on the sum frequency can be separated from the bias terms in the spatial frequency domain. To accomplish this, we set $u_o = (v_2 - v_1) / v_o$. We write the product of the cosines as a sum, and the term of interest in Eq. (B1) takes the following form:

$$\begin{aligned} Q(\tilde{x}, \tilde{y}) = & (Bv_o \tau r_o / 2) \operatorname{sinc} \left[(br / \pi v_o) (\tilde{x} - 2R_o v_o / c) \right] \\ & \times \sum_n^N A(nT) \cos \left[4\pi u_o \tilde{x} - \pi b_2 \tilde{y}^2 / \tilde{x} \right. \\ & \left. + 2\pi b_2 (n-N)\Delta y \tilde{y} / \tilde{x} - \pi b_2 \Delta y^2 (n-N)^2 / \tilde{x} + 2\pi v_o v^2 T^2 n^2 / c R_o \right. \\ & \left. - 4\pi v_o n T \eta_o c R_o + 2\pi v_o \eta_o^2 / c R_o + \phi \right]. \quad (B2) \end{aligned}$$

The focusing of the SAR image in the azimuth direction (η) is accomplished by the summation over n in the above equation. The summation will result in a well-focused image in the \tilde{y} direction if the terms containing n^2 in the argument of the cosine are canceled. To accomplish this, the constant b_2 of the mask is set appropriately.

$$\begin{aligned} (2v_o v^2 T^2 / c R_o) n^2 = & (b_2 \Delta y^2 / \tilde{x}) n^2 - \\ - b_2 = & \frac{2v_o v^2 T^2 \tilde{x}}{c R_o} = \frac{2v_o v^2 T^2}{c R_o} (2R_o v_o / c) \\ = & \frac{4v_o v^2 T^2 v_o}{c^2 \Delta y^2}. \quad (B3) \end{aligned}$$

Equation (B3) and the value we previously chose for u_o provide all the information necessary to construct the mask that is used in the system. Equation (B3) is substituted in Eq. (B2), and all inconsequential phase terms are included in the parameter ϕ . Equation (B2) then reduces to the following equation:

$$\begin{aligned} Q(\tilde{x}, \tilde{y}) = & (Bv_o \tau r_o / 2) \operatorname{sinc} \left[(br / \pi v_o) (\tilde{x} - 2R_o v_o / c) \right] \\ & \times \sum_n^N A(nT) \cos \left[4\pi u_o x + (4\pi v_o v^2 T^2 / c \Delta y R_o) \right. \\ & \left. \times (\tilde{y} - (\eta_o \Delta y / v T) + N\Delta y) n + \phi \right] \quad (B4) \end{aligned}$$

The summation over n in Eq. (B4) is recognized as the discrete cosine transform¹² of the antenna pattern $A(nT)$. In order to get an approximate result, we can assume that the antenna pattern is so broad in the azimuth direction that its main lobe uniformly illuminates a distance $v_n T$ on the ground. Therefore, $A(nT)$ is approximately a constant for $0 > n > N$, and Eq. (B4) can be evaluated as follows¹³:

$$\begin{aligned} Q(\tilde{x}, \tilde{y}) = & (Bv_o \tau r_o / 2) \operatorname{sinc} \left[(br / \pi v_o) (\tilde{x} - 2R_o v_o / c) \right] \\ & \times \frac{\sin \left[(2N\pi v_o v^2 T^2 / c \Delta y R_o) (\tilde{y} - (\eta_o \Delta y / v T) + N\Delta y) \right]}{\sin \left[(2\pi v_o v^2 T^2 / c \Delta y R_o) (\tilde{y} - (\eta_o \Delta y / v T) + N\Delta y) \right]} \\ & \times \cos (4\pi u_o x + \phi). \quad (B5) \end{aligned}$$

The ratio of the sines in Eq. (B5) can be approximated by a sinc function for large N , and this leads us to the final form of Eq. (15):

$$\begin{aligned} Q(\tilde{x}, \tilde{y}) = & (NBv_o \tau r_o / 2) \operatorname{sinc} \left[(br / \pi v_o) (\tilde{x} - 2R_o v_o / c) \right] \\ & \times \operatorname{sinc} \left[(2Nv_o v^2 T^2 / c \Delta y R_o) (\tilde{y} - (\eta_o \Delta y / v T) + N\Delta y) \right] \\ & \times \cos (4\pi u_o x + \phi). \quad (15) \end{aligned}$$

9. REFERENCES

1. D. A. Ausherman, *Opt. Eng.* 19(2), 157(1980).
2. T. M. Turpin, *Proc. IEEE* 69(1), 79(1981).
3. W. T. Rhodes, *Proc. IEEE* 69(1), 65(1981).
4. E. N. Leith, *Proc. IEEE* 59(9), 1305(1971).
5. I. Cindrich, J. Marks, and A. Klooster, *Proc. SPIE* 128, 128(1977).
6. A. Korpel, *Proc. IEEE* 69(1), 48(1981).
7. K. Bromley, M. Monahan et al., *Proc. SPIE* 118, 118(1977).
8. M. Blouke et al., *Proc. SPIE* 290, 6(1981).
9. D. Casasent, *Proc. IEEE* 65, 143 (Jan. 1977).
10. J. Hall, in *Applied Optics and Optical Engineering*, Vol. VIII, Chap. 8, Academic Press, New York (1980).
11. D. Psaltis and K. Wagner, *Proc. SPIE* 271, 51(1981).
12. A. W. Rihaczek, *Principles of High Resolution Radar*, McGraw Hill, New York (1969).
13. A. Oppenheim and R. Schaffer, *Digital Signal Processing*, Prentice Hall, Englewood Cliffs, New Jersey (1975).

REAL TIME SYNTHETIC APERTURE RADAR PROCESSING*

Demetri Psaltis, Michael Haney and Kelvin Wagner
Division of Engineering and Applied Science
California Institute of Technology
Pasadena, California 91125

ABSTRACT

Real time acousto-optic SAR processors are described and experimentally demonstrated. SAR imaging is performed in one of the architectures by applying the signal to an acousto-optic device and correlating it with chirp signals recorded on an optical transparency by time integration on a CCD detector. In a different implementation, the imaging is performed by interfering the light beams diffracted from two separate acousto-optic devices, one modulated by the radar signal and the second by the reference chirp waveform.

INTRODUCTION

Synthetic Aperture Radar [1,2] is a powerful technique for the formation of high resolution images at long wavelengths. The most attractive feature of the technique is the fact that the resolution is not limited by the physical aperture of the receiving antenna, but the bandwidth of the radar and the distance the vehicle carrying the antenna travels while each point of the object being imaged remains illuminated by the radar. Therefore, SAR images of the earth can be formed with excellent resolution by aircraft or spacecraft that can carry only small antennas. Until recently, the usefulness of the technique has been limited to applications that do not require real time image formation because of the high computational load associated with forming the focused image from the received radar signals. Typically, the radar returns are recorded on the aircraft or spacecraft carrying the radar and the images are formed later on the ground by optical or digital computers. The requirements of modern radars and advances in signal processing technologies have raised the possibility of producing SAR images in real time on-board the vehicle carrying the radar. Such capability would enhance significantly the applicability of the SAR imaging method. The advances in the state-of-the-art of digital and optical signal processing technologies that have been accomplished in recent years make it possible to form SAR images in real time. Processing speed however is only one of the requirements for a practical SAR processor. Factors such as power consumption, weight, size, cost and flexibility are also very important. The optical implementation is at a relative disadvantage to a digital implementation with respect to flexibility and accuracy, but low power consumption, size/weight and cost make the optical implementation the only practical solution in many SAR imaging applications.

*This research is supported by NASA through the Jet Propulsion Laboratory, by the Air Force Office of Scientific Research and by General Dynamics. M. Haney is attending Caltech on a corporate sponsored Ph.D. fellowship from General Dynamics.

We have described recently [3,4] an optical architecture for SAR imaging that is implemented with an acousto-optic device (AOD) as the input transducer and a 2-D CCD detector array on which the SAR image is formed. In this paper the principles of operation of this architecture are reviewed and experimental demonstration of real time SAR imaging is presented. A new interferometric architecture is also presented in which the impulse response of the system is controlled with a second AOD that is modulated by a chirp waveform. The new architecture provides the flexibility of dynamically adapting the parameters of the optical processing to track changes in the radar geometry.

EXPERIMENTAL PROCESSOR

We will present the operation of the processor by describing how it produces a focused image of a point target. A focused SAR image is related to the reflectivity of the area being imaged through a 2-D linear operation. Therefore the impulse response describes the system completely. The typical side-looking SAR geometry is shown in Figure 1. An airplane flying at a constant velocity v_a parallel to the ground, illuminates an area on the ground through a small antenna mounted on the side of the aircraft. The illuminating radiation is temporally modulated by periodic linear FM pulses. The transmitted waveform is given by the following expression.

$$s(t') = \sum_n \text{rect} \left[\frac{(t' - nT)}{\tau_0} \right] \exp [jb_1 (t' - nT)^2] \exp (j\omega_0 t'). \quad (1)$$

t' is time, $1/T$ is the pulse repetition frequency (PRF), τ_0 is the duration of each pulse, b_1 is the chirp rate and $\omega_0/2\pi$ is the center frequency of the radar. The single point scatterer on the ground scatters the illuminating field and part of it is detected by the antenna on the aircraft. For a single point scatterer the received waveform is a replica of what was transmitted delayed by $2R/c$, where R is the distance from the antenna to the scatterer and c is the speed of light. R changes with time as the aircraft flies by the target and from Fig. 1 we find that $R(t') = (R_0^2 + x^2)^{1/2} = [R_0^2 + v_a^2 (t' - t_0)^2]^{1/2} = R_0 (1 + v_a^2 (t' - t_0)^2 / 2R_0^2)$, where R_0 is the distance to the scatterer at the time $t' = t_0$ when the vehicle crosses over the scatterer and the assumption has been made that $R_0 \gg x$. Typically the variation of $R(t')$ during the time the scatterer is illuminated is small enough and it does not affect the time of arrival or the chirping rate of the received pulses. Therefore each pulse is received with approximately the same delay, $2R_0/c$. This delay is measured by compressing the received pulses and the image of the scatterer is focused in this manner in the across track (or range) dimension. The variation of R appears as a phase shift on the received waveform. This phase modulation is then used to focus the image in the along track (or azimuth) direction. With these assumptions and ignoring the effects of the antenna pattern, the received waveform can be written as follows.

$$s(t' - R(t')) = \sum_n \text{rect} \left[\frac{(t' - 2R_0/c - nT)}{\tau_0} \right] \exp [jb_1 (t' - 2R_0/c - nT)] \\ \times \exp (j\omega_0 t') \exp [j\omega_0 v_a^2 (nT - t_0)^2 / R_0]. \quad (2)$$

It is customary to think of this long 1-D signal as a 2-D unfocused image of the ground. We define $\tau = t' - nT$ and $t = nT$ and we write the received signal as a 2-D function as follows.

$$s(\tau, t) = \text{rect} \left[\frac{\tau - 2R_0/c}{\tau_0} \right] \exp [jb_1 (\tau - 2R_0/c)^2] \\ \times \exp [j\omega_0 v_a^2 (t - t_0)^2 / R_0] \exp [j\omega_0 \tau]. \quad (3)$$

The above 2-D function is in general a non-symmetric zone plate whose center ($\tau = 2R_0/c$, $t = t_0$) is proportional to the position of the point scatterer on the ground. In the optical processor to be described this signal is focused by spatial integration in the range (τ) direction. The variable t does not represent the continuous time. It is a discrete time variable sampled at the radar PRF. We will refer to it as simply time in the rest of our discussion. In order to characterize and demonstrate the operation of the real time SAR processor, we have built an apparatus that generates the impulse response signal of Eq.(3). A schematic diagram of the impulse response generator is shown in Fig. 2. The frequency of a 10 MHz oscillator is divided by a factor of 2×10^4 to produce a phase locked PRF clock at 500 Hz. The same 10 MHz frequency is used to derive a 60 MHz signal and this signal is then applied to a digitally controlled phase shifter. The phase shifter is addressed by a read-only memory circuit in which a quadratic function is stored. The quadratic function stored in the memory is displayed in Fig. 3. This was obtained through a D/A converter. The memory chip is read-out at the PRF of the radar and consequently the signal following the phase shifter has a slow linear frequency modulation (20 Hz/frame in the experiments presented later) simulating the t variation of the signal in Eq. (3). The PRF clock triggers a circuit that produces a very short pulse (16.6 nseconds) which is in turn mixed with the phase shifted 60 MHz carrier and applied to a surface acoustic wave device. The dispersive properties of the SAW device cause the impulses to be spread in time to 6 useconds and in frequency to the range 50 to 70 MHz. The SAW introduces in this manner the τ modulation of the signal in Eq. 3. The output of the SAW is a replica of the signal of the signal that is received by a synthetic aperture radar illuminating a scene containing only one point reflector. This signal is displayed by mixing it to base-band and modulating the intensity (z axis) of an oscilloscope. The horizontal (x) amplifier of the oscilloscope is triggered by the PRF clock and the vertical axis is deflected by a slow ramp. Fig. 4 shows the 2-D zone plate produced by the system described above. This zone plate is a representation of the unfocused image of a point scatterer.

The signal from the impulse response generator is applied to an AOD. A shear wave TeO_2 device was used in the experiments with 70 μsec delay window and 30 MHz (40-70 MHz) 3dB bandwidth. The AOD is illuminated by a pulsed laser diode. The

laser pulses are produced at the radar PRF and they are synchronized to occur when the acoustic signal in the AOD consists of a single chirp generated by the SAW device. The duration of each laser pulse is shorter than the inverse of the bandwidth of the chirp signals and consequently the motion of the travelling acoustic wave does not affect the operation of the processor. A single mode AlGaAs laser was used in the experiment, at 15mW peak power and 30 nanoseconds pulse width. The chirped signal forms a phase grating in the AOD with linearly increasing spatial frequency. This is shown in Fig. 5. The light diffracted near the piezoelectric transducer of the AOD in Fig. 5 is diffracted at a larger angle than the light diffracted from the top of the device. Consequently, the diffracted light comes to a focus. The focal plane is located 11.5 cm away from the AOD in the experiment and at this point the diffracted light is well separated from the zero beam and it can be detected. The self-focusing of the diffracted light accomplishes the focusing of the SAR image in the range (τ) direction. The optical field at the plane where the diffracted light comes to focus is given by

$$\begin{aligned} S_1(x,t) &= \int S(x'/v,t) \exp[-jb_1(x'+x)^2/v^2] dx' \\ &= \text{Sinc}[(x-2R_0 v/c) \tau_0 b_1/\pi v^2] \exp[j\omega_0 v_a^2(t-t_0)^2/cR_0 + j\omega_0 \tau], \end{aligned} \quad (4)$$

where x' and x are the spatial co-ordinates in the plane of the AOD and the detector respectively. v is the acoustic velocity. The range focused signal is phase modulated in t by the azimuth chirp. This phase modulation can only be detected interferometrically. Interferometric detection is accomplished by adding a 60 MHz sinusoid to the radar signal and applying the sum to the AOD. The sinusoid will cause a plane wave to be diffracted in the same direction as the focusing signal beam. The light intensity at plane x is given by

$$\begin{aligned} I_1(x,t) &= |S_1(x,t) + \exp(j\omega_0 \tau)|^2 = \\ &= 1 + \text{sinc}^2[(x-2R_0 v/c) \tau_0 b_1/\pi v^2] + 2 \text{sinc}[(x-2R_0 v/c) \tau_0 b_1/v^2] \\ &\quad \times \cos[\omega_0 v_a^2(t-t_0)^2/R_0 c]. \end{aligned} \quad (5)$$

The SAR image is focused in the azimuth (t) direction by correlating the time variation of the above function with the function $\cos(\omega_0 v_a^2 t^2/R_0)$. This is accomplished with a time integrating optical correlator, a simple diagram of which is shown in Fig. 6. A transparency with intensity transmittance $I_2(y) = 1 + \cos(b_2 y^2)$ is illuminated with light whose intensity is temporally modulated by $I_1(x,t)$. y is the spatial co-ordinate perpendicular to x . The light is detected after the transparency on a 2-D detector. For the purpose of this discussion we can think of the detector as photographic film. If the film travels with velocity v' in the y

direction while it is exposed to light, the detected signal on the film is $I_3(x,y) = \int I_1(x,t) I_2(y+vt) dt$. We choose the parameter $b_2 = \omega_0 v_a^2 / R_0 v'^2$ and the signal accumulated on the detector becomes the autocorrelation of the linear FM waveform in Eq. (5).

$$I_3(x,y) = 1 + \text{sinc}^2 [(x-2R_0 v/c) \tau_0 b_1 / \pi v^2] \\ + 2 \text{sinc} [(x-2R_0 v/c) \tau_0 b_1 / \pi v^2] \text{sinc} [(y-t_0 v') b_2 Y / \pi] \quad (6)$$

where Y is the total distance the moving detector travels.

The first term in Eq. (6) is a constant bias, the second is a signal dependent bias term and the third term is the focused SAR image. The image can be separated from the bias terms using one of several possible methods. For instance the bias alone can be calculated separately on a different detector and then subtracted from $I_3(x,y)$ to produce an unbiased image. Alternatively the signal term in Eq. (6) can be formed on a sufficiently high spatial frequency in either x or y and separated from the bias terms by electronic filtering.

The detector used in the processor is a 2-D CCD. The photogenerated charge stored in a CCD can be made to travel along one of the spatial dimensions by applying pulse waveforms to the device. The charge travels in discrete steps but this is actually convenient for this system since t is a discrete time variable as well. The motion of the photogenerated charge is entirely equivalent to the physical movement of the detector in Fig. 6. Therefore the CCD performs the correlation in the azimuth direction by time integration. The appropriate value for the velocity v' is set by transferring the change pattern on the CCD by one pixel at the radar PRF.

The CCD used in our experiments has 512 pixels in the direction of charge motion and 320 in the other dimension. The entire SAR processor, shown in Fig. 7, is constructed by cascading the space integrating range processor of Fig. 5 and the time integrating processor of Fig. 6. A photograph of the experimental set-up is shown in Fig. 8. The mask used as the azimuth reference is shown in Fig. 9. This mask was generated with a computer controlled film recorder. Notice that the chirping rate in the vertical direction is dependent on the horizontal (range) position. This is necessary for compensation of the range azimuth coupling (the focal length along the azimuth direction of the zone plate in Fig. 4 depends on the range of each target). A photograph of the focused SAR image produced in real time with the processor in Fig. 8 from the signal displayed in Fig. 4 is shown in Figure 10a.

The image obtained is that of the single point scatterer. The dimensions of this focused spot along the horizontal (range) and vertical (azimuth) directions determine the resolution of the SAR processor. The width of the spot in the horizontal direction is expected to be equal to the acoustic velocity divided by the bandwidth of the chirp (20 MHz) produced by the SAW device [3]. The width of the spot in Fig. 10a is broader than expected by a factor of two. We attribute this to apodization due to the gaussian shape of the wavefront illuminating the AOD and possibly aberrations in the lenses. The number of pixels that the spot is expected

to occupy in the vertical (azimuth direction) is equal to the total number of pixels of the CCD in the vertical direction (512) divided by 40 (the time-bandwidth product of the azimuth chirp). The measured spot width is approximately equal to what is expected in the azimuth direction. The isometric display of the focused image (shown in Fig. 10b) reveals the structure of the bias on which the image is formed. There is a flat plateau due to the collimated reference wave and for this case of a single point target an additional ridge along the azimuth direction (the second term in Eq. 3). The sidelobe structure of the focused spot can be observed in the cross sectional scan (along the azimuth direction), shown in Figure 10c. In Figs. 10b and 10c the compression in the azimuth direction is 80 (2 times more than in Fig. 10a). The digital simulation of the autocorrelation of a linear FM waveform with a time-bandwidth product equal to 80 (displayed in Fig. 40d) shows that the level and the structure of the optically produced sidelobes are remarkably accurate. The sidelobe level can be reduced further by apodization and/or increasing the pulse compression ratio in the azimuth direction. The value 80 for azimuth pulse compression we used in the experiment is typical for aircraft radars.

ADAPTABLE ARCHITECTURE

In some applications the parameters of the radar such as the velocity and the altitude of the aircraft and the direction in which the antenna is pointed (side looking, forward looking, spotlighting) change dynamically. Consequently, the real time SAR imager must have the capability of adapting rapidly to such changes in order to continuously produce a well focused image. The impulse response of the processor described in the previous section is determined in part by the transmittance of the mask used. A real time spatial light modulator can be used in place of the mask. Since the transmittance of such a device can be changed dynamically, the impulse response of the processor can be adapted to match the radar parameters. An alternate and preferable approach is to use a second AOD in place of the fixed mask. The mask, as we see in Fig. 9, introduces a 2-D spatial light modulation. The modulation along one of the dimensions however is simply scaling. Therefore the AOD, which is a 1-D spatial light modulator, can be used to introduce the basic chirp modulation in the y direction. An optical system that images the AOD along the y direction with different magnification for each x position produces a 2-D spatial light distribution, which when detected interferometrically, results in a pattern identical to the one shown in Fig. 9. This is shown schematically in Fig. 11. A cylindrical lens L_1 is used to focus the light in the AOD and L_2 recollimates the diffracted light. The lens L_3 is a cylinder that has focusing power in the vertical direction. Let us assume that the AOD is modulated by a single frequency. The diffracted light in this case is a plane wave and it will be focused to a horizontal line by the cylindrical lens L_3 . L_3 is rotated around a pivot coinciding with the y axis by an angle θ . The focused line lies in the (x,z) plane and it is at an angle θ with respect to the x axis. The light propagates as a diverging tilted cylindrical wave after the focal plane of L_3 . If we observe interferometrically this light distribution in a plane P_2 perpendicular to the z axis, we will see the pattern shown in Fig. 4. If the interference of the output of the systems in Figs. 5 and 11 is formed on the CCD, the detected signal will be exactly the same as the signal in Eq. 5. It is interesting to note that the tilted cylindrical lens alone is sufficient to produce the desired interference pattern. The AOD however provides added flexibility in several respects. The chirping rate and the starting frequency of the azimuth reference can be

dynamically controlled by modulating the AOD with the appropriate temporal waveform. Furthermore, the azimuth correlation can be formed by shifting the signal in the AOD instead of transferring the charges in the CCD. This capability is useful for producing multiple looks, i.e., forming independently several images of the same area and adding them to reduce speckle. If the charge pattern in the CCD is travelling during exposure, the focused images are continuously read-out and therefore it is not possible to add on the detector multiple looks. Finally the use of the AOD allows us to build the architecture as a cascade of the systems in Figs. 5 and 11, rather than a two-arm interferometer. This is an important consideration when we consider the mechanical stability of the system. The cascaded architecture is shown in Fig. 12. In this architecture all beams go through the same optics. In order to record a chirp signal on the detector we must interfere two waves with different degrees of collimation. The second AOD in Fig. 12 is modulated by the sum of a single sinusoid and a chirp signal. The light diffracted by this AOD consists of a plane wave and a diverging spherical wave and thus the interference of these two diffracted waves after lens L_4 produces fringes with linearly increasing spatial frequency in the y direction, as desired.

REFERENCES

- [1] E. N. Leith, Proc. IEEE, 59, 1305 (1971).
- [2] I. Cindrich, J. Marks and A. Klooster, Proc. SPIE, 128, 128 (1977).
- [3] D. Psaltis and K. Wagner, Optical Engineering, 21, 822 (1982).
- [4] D. Psaltis, K. Wagner and M. Haney, Soc. Photo. Opt. Inst., Eng., 352, San Diego, CA, 1982.

ACKNOWLEDGMENT

We thank T. Bicknell for numerous helpful discussions and J. Yu for his assistance in the experiments.

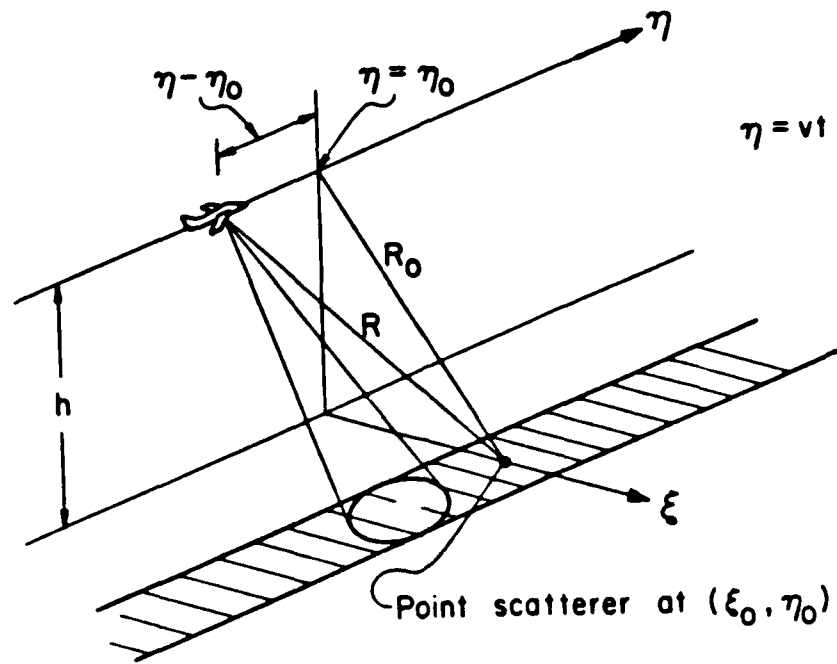


Figure 1. Synthetic Aperture Radar Geometry

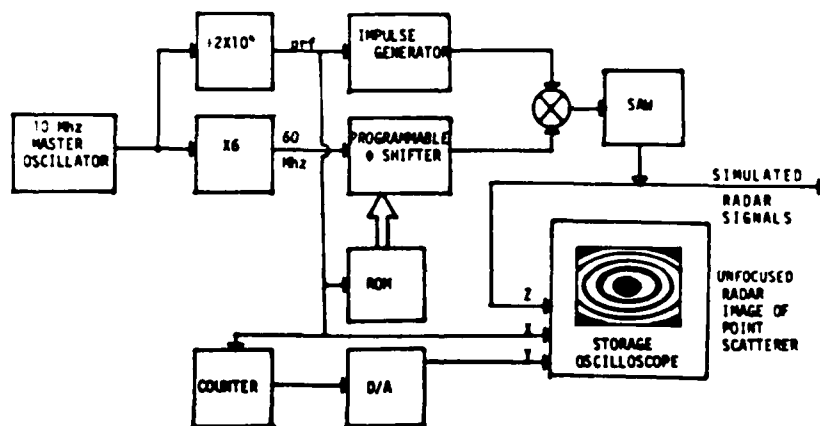


Figure 2. SAR impulse response simulator

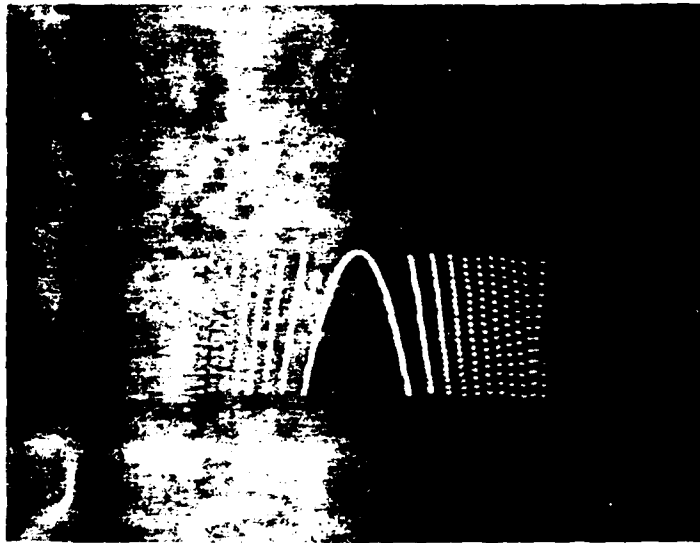


Figure 3. Quadrature phase modulation simulating the phase history.

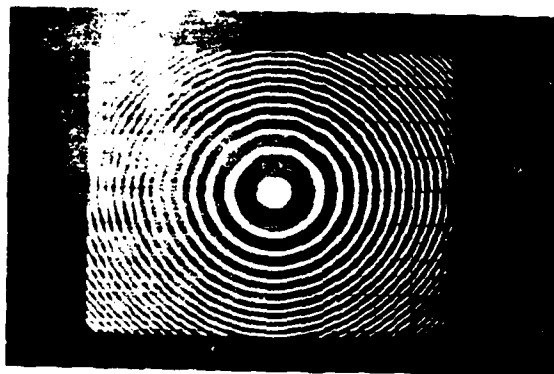


Figure 4. Simulated SAR impulse response produced in real time by the system in Figure 2.

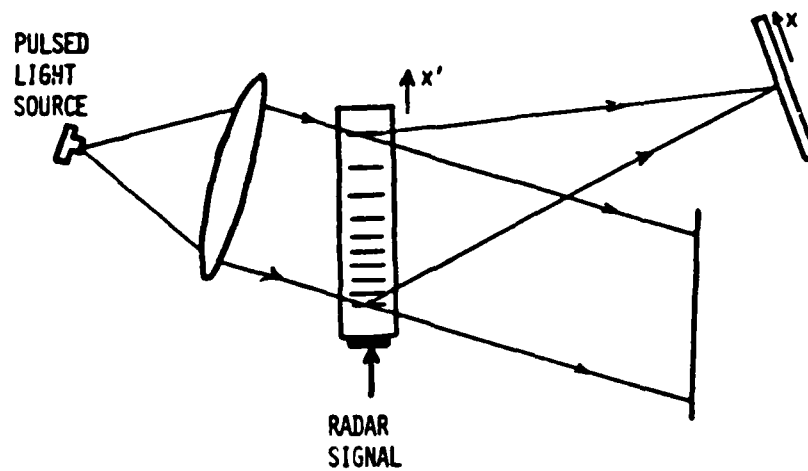


Figure 5. Acousto-optic processor that performs the focusing of the SAR image in range.

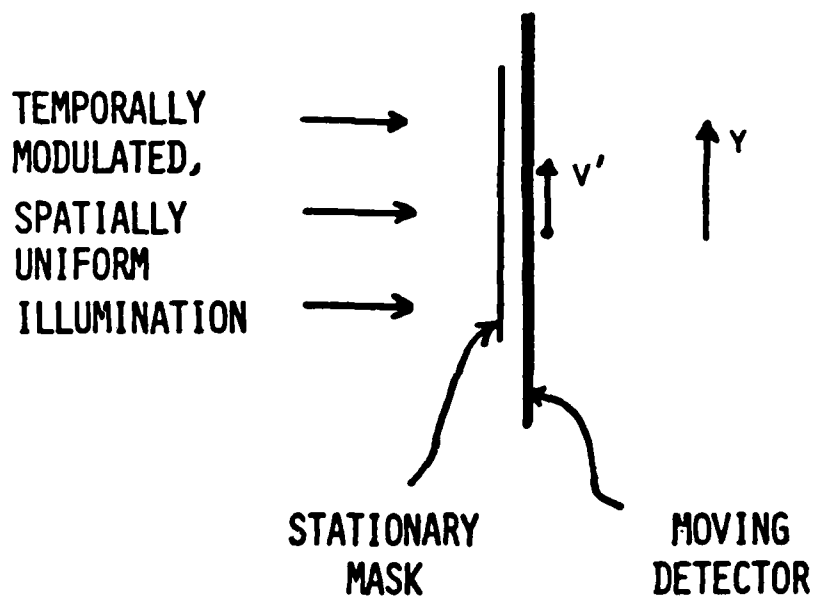


Figure 6. Time integrating optical processor that performs the focusing of the SAR image in azimuth.

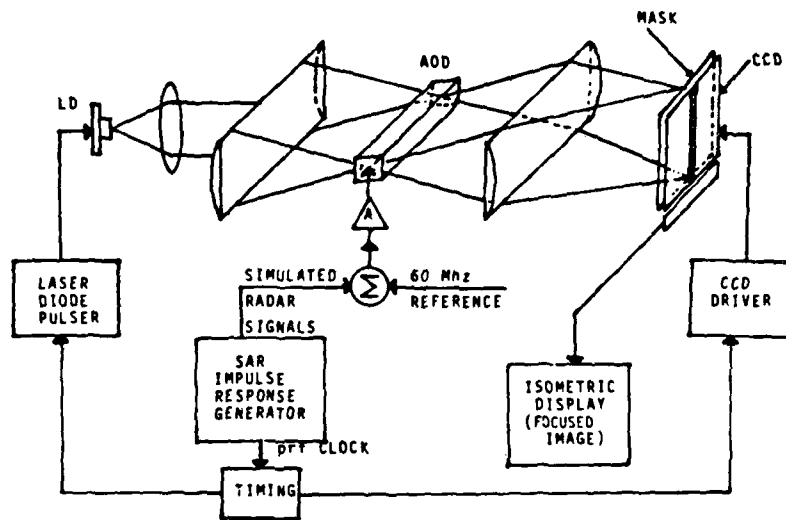


Figure 7. Schematic diagram of the overall real-time SAR processor.

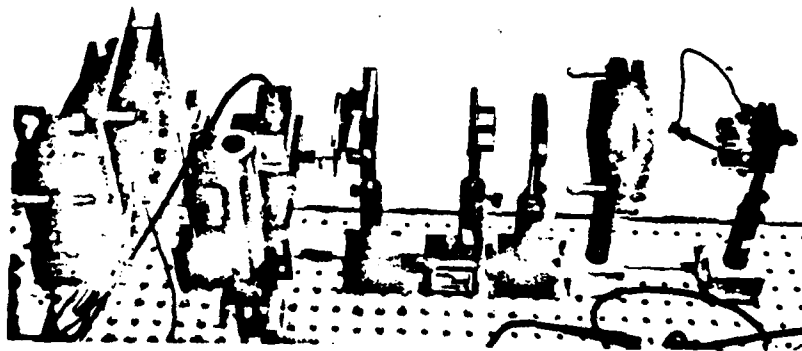


Figure 8. Experimental SAR processor.

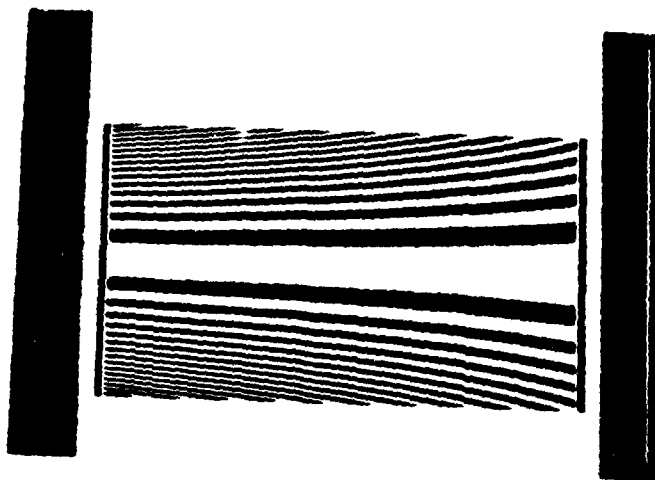


Figure 9. Computer generated mask used in the processor of Figure 8.

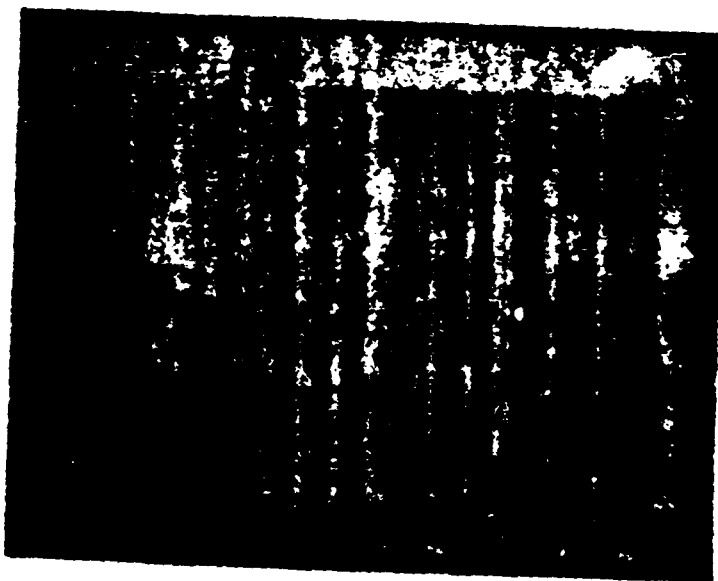
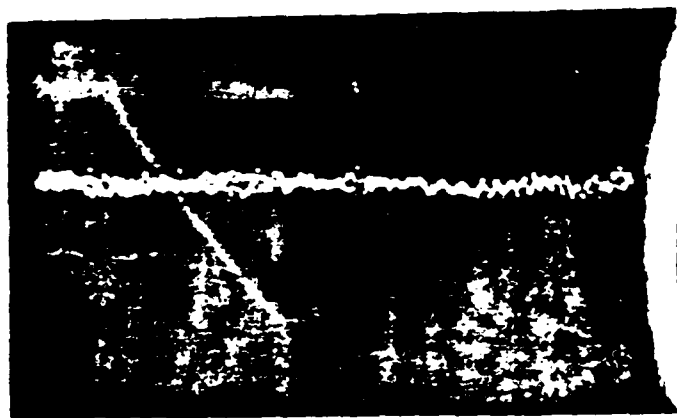
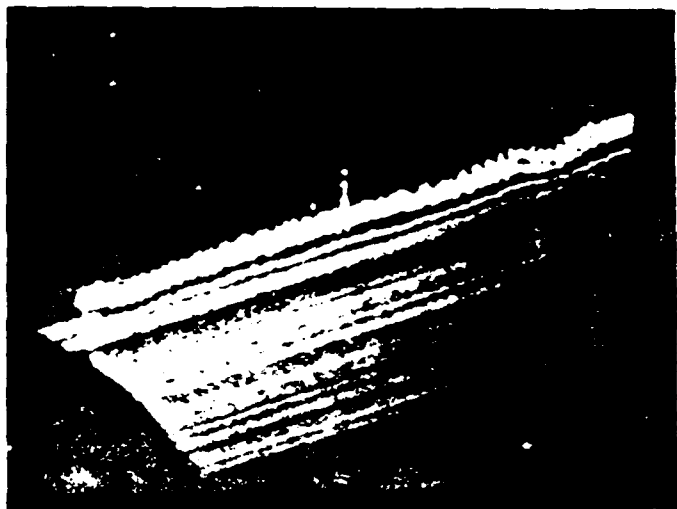


Figure 10a. Focused SAR image of the single point scatterer corresponding to the zone plate in Figure 4, produced in real-time with the processor of Figure 8.



RUN

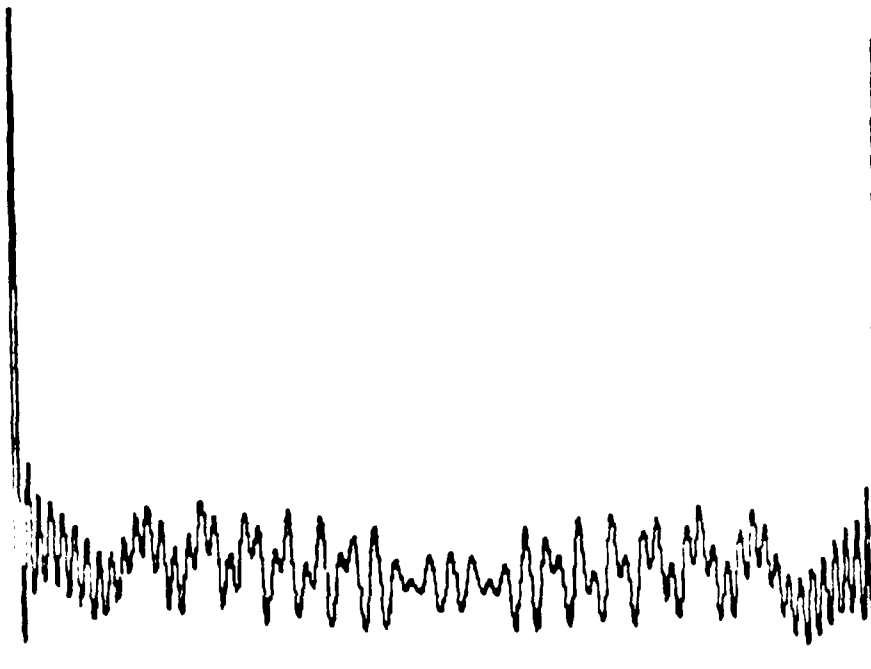


Figure 10b. Isometric display of the focused point scatterer demonstrating the bias structure.

10c. Cross sectional scan in azimuth showing the sidelobe structure. (pulses compression)

10d. Digital simulation of the signal shown in Figure 10c.

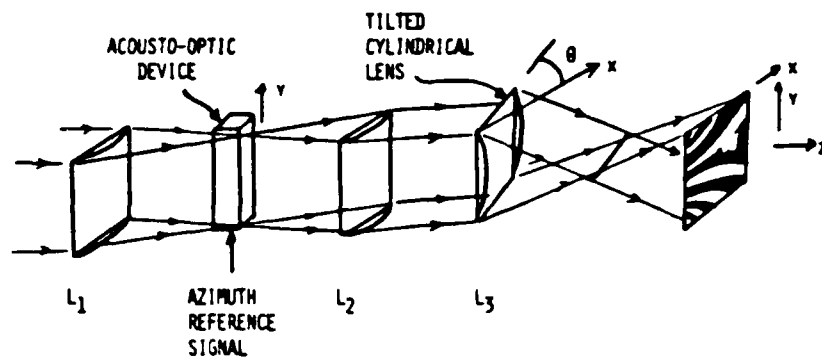


Figure 11. Acousto-optic system with which the azimuth reference is interferometrically introduced.

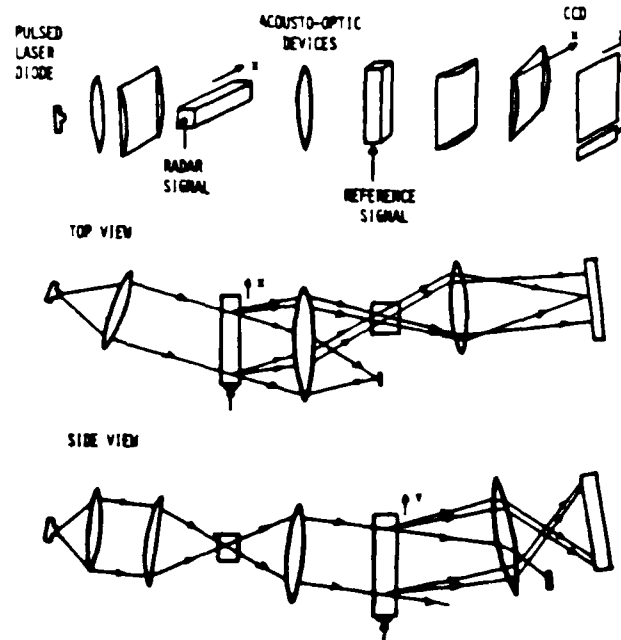


Figure 12. Optical architecture for SAR imaging with the azimuth reference introduced through a second AOD in place of the mask used in Figure 7.

REAL-TIME SYNTHETIC APERTURE RADAR IMAGE
FORMATION UTILIZING AN ELECTROOPTIC SPATIAL
LIGHT MODULATOR

I. Abramov, Y. Owechko, and A.R. Tanguay, Jr.
Departments of Electrical Engineering
and Materials Science,
and Image Processing Institute
University of Southern California
Los Angeles, CA 90089-0483

and

T.J. Bicknell
Jet Propulsion Laboratory
California Institute of Technology
Pasadena, CA 91109

In the process of synthetic aperture radar data acquisition, each point target in the terrain to be imaged is illuminated by numerous consecutive radar pulses during an azimuthal terrain traverse by the radar platform (typically aircraft or space vehicles). Thus a given point target contributes a return signal that mimics the radar pulse shape, at a time delay that depends on the point target range at each radar platform azimuth, and at a center frequency Doppler-shifted by the instantaneous relative velocity of the platform with respect to the target. Recovery of the point target location and scattering strength from such a two-dimensional (range and azimuth) signal record is exceedingly complex, since the return signal amplitude at any given time is comprised of scattered components from

all points in the illuminated terrain.

The image formation algorithm from synthetic aperture radar data involves the two-dimensional deconvolution of the recorded phase and amplitude history of the radar return from the radar pulse shape in the range dimension, and from the Doppler-induced phase modulation in the azimuth dimension. For ease in digital processing using fundamentally sequential architecture machines, the two-dimensional deconvolution is typically replaced by two one-dimensional deconvolutions in the azimuth and range dimensions. The reference function utilized in the azimuth deconvolution is a function of range, and hence is inherently space-variant. Since the reference functions employed typically require of order 1000 sampled elements to maintain high resolution in the reconstructed image, such computations are quite cumbersome and often prohibitive.

Optical reconstruction of synthetic aperture radar images can be readily accomplished by recording the return signal phase history on an image storage device such as photographic film. The two-dimensional amplitude that results from a given point target forms a zone plate that is self-focusing in both dimensions when coherently illuminated. Since the azimuth and range focal lengths are functions of distinct parameters, they must in general be brought into coincident focus by cylindrical lenses oriented to act separately on the range and azimuth dimensions.

A number of advantages accrue to such optical SAR processors

due to the inherent parallelism of the optical processing algorithm. The inherent speed advantage allows real-time systems to be envisioned that are small, lightweight, and low-power. Although digital processors are usually characterized by superior computational accuracy, they are typically quite large, expensive, and power consumptive. Many radar applications such as quick-look or search modes require or would be better served by on-board processing. These SAR systems will require small, lightweight processors, especially for use in conjunction with spacecraft-borne radars.

Present implementations of coherent optical SAR processors share a common limitation, in that real-time operation is obviated by the use of photographic film as an incoherent-to-coherent image transducer. One possible approach to high speed optical synthetic aperture radar signal reconstruction involves the utilization of two-dimensional real time spatial light modulators as recycleable replacements for photographic film in the input transducer plane of modified SAR coherent optical processors, as shown in Figure 1. Leading candidate spatial light modulators include the Pockels Readout Optical Modulator (PROM), CCD-addressed liquid crystal light valves, and CCD-addressed membrane light modulators. The fundamental physical limitations of such real time devices that affect SAR processor performance characteristics are under investigation. Current research on the PROM is focused on the effects of device operational mode, device constitutive parameters, electrooptic crystal orientation, writing wavelength, frame rate/data overwrite/

2-D SPATIAL LIGHT MODULATOR CORRELATOR

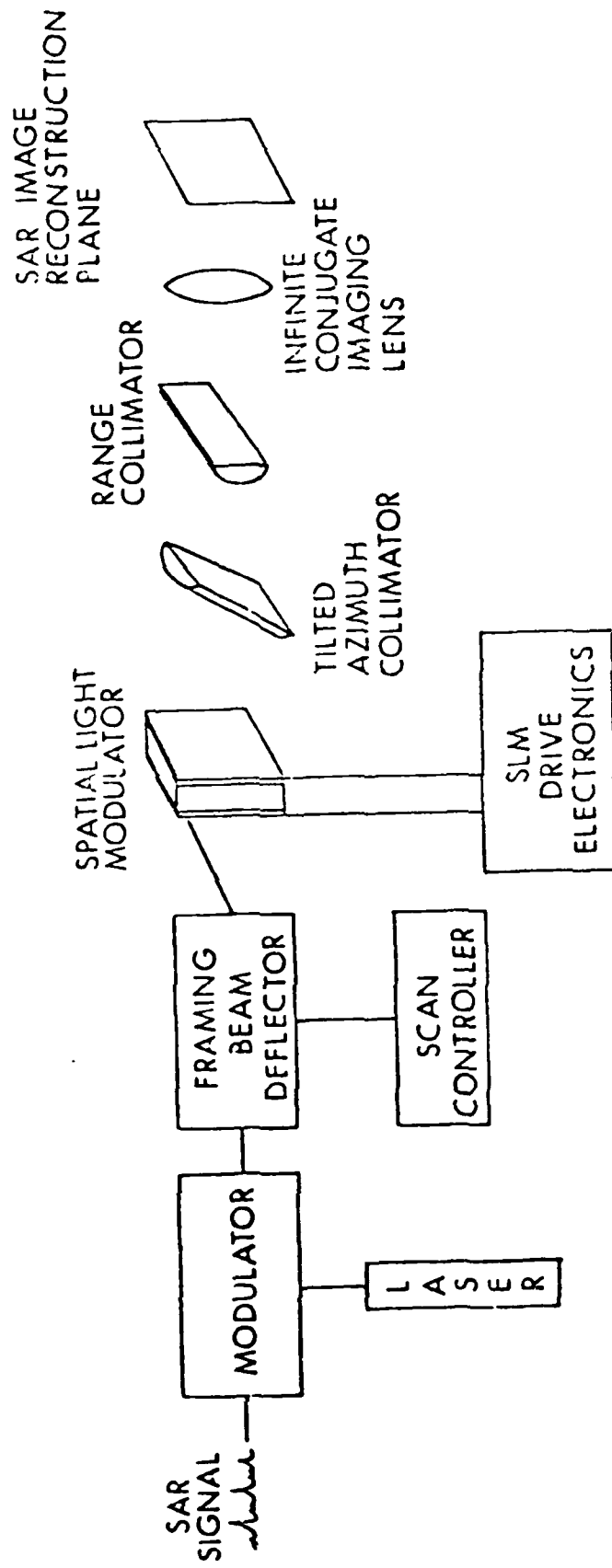


Figure 1: Coherent optical synthetic aperture radar processor utilizing an Electrooptic Spatial Light Modulator.

presumming, erasure completeness and image retention on the overall quality of SAR image formation.

Several modes of addressing such two-dimensional spatial light modulators are under active consideration, including a z-axis modulated x-y laser scanner, an image-intensified CRT display, and an acousto-optic delay line. A promising new device, the Xerox Linear Array Total Internal Reflection spatial light modulator, is under development and evaluation for the page composition function.

The recent development of such novel electrooptic spatial light modulators (both one- and two-dimensional) will allow real-time coherent optical SAR processors to be implemented. It is hoped that the availability of such processors will initiate new mission applications not presently envisioned due to current digital processor limitations.

END

FILMED

MARCH, 19 88

DTIC